Description of the PlankTOM12.2 equations

Erik Buitenhuis, Joe K. Guest, Rebecca M. Wright,
Philip Townsend and Corinne Le Quéré

September 2023

Contents

1 Introduction

This Supplement presents a full description of the PlankTOM model, a global marine biogeochemical model based on the representation of twelve Plankton Functional Types (PFTs), including six phytoplankton (pPFTs), five zooplankton (zPFTs) and bacteria. PlankTOM also represents the full cycles of C, O_2, P and Si and simplified cycles for Fe and N. This version comprises of 41-51 biogeochemical tracers (Table 1).

1.1 Notation

In the following sections, we will show the equations governing tracer and food-web dynamics. These equations are mostly semi-empirical, and have been developed and tested using a multitude of laboratory and field data. As long as not otherwise indicated, both tracers and their respective concentrations will be designated by capital letters, with

- P_i: concentration of pPFT$_i$ with $i \in \{1, 6\}$,
- Z_j: concentration of zPFT$_j$, with $j \in \{1, 5\}$,
- F_k: concentration of food k; where F_k includes phytoplankton and other food sources
- PRO: proto-zooplankton concentration,
- NO3: concentration of nitrate, etc.

All concentrations are calculated in $\frac{mol}{L}$ except for PO_4, which is in $\frac{molC}{L}$, chlorophyll, which is in $\frac{gCHL}{L}$, and alkalinity, which is in $\frac{equivalent}{L}$.

Tables and an index are provided which link the mathematical symbols with the variable names used in the Fortran code. Where subscript j includes pico-heterotrophs in addition to the zoo-plankton types this is stated explicitly.

The plankton functional types and the tracers are shown in Figure 1. Figures of this type showing the processes governing the evolution of the PFTs and tracers are included in the following sections.

1.2 Tracer Transport

The temporal evolution of all passive tracers T is governed by the balance between its local sources and sinks ('Sources-Minus-Sinks' (SMS), biogeochemical part) and by the physical transport processes (advection and diffusion), hence

$$\frac{dT}{dt} = \nabla \cdot (\vec{u}T) + \nabla \cdot (\vec{K}\nabla T) + SMS, \tag{1}$$

where $\vec{K}$ is the 3-dimensional tracer diffusion coefficient and $\vec{u}$ is the fluid velocity, calculated in the physical model.

To ensure numerical stability, the sinks processes in SMS are set to zero then the concentration of passive tracers fall below a set threshold (1.e-10).

Table 1: List of biogeochemical Tracers in PlankTOM

Abbreviation	**Description**	**Units**
ALK	alkalinity	eq L^{-1}
ARA	aragonite	mol L^{-1}
B14B	bomb 14C	mol L^{-1}
BAC	pico-heterotrophs	mol L^{-1}
BFE	Fe in large POM	mol L^{-1}
BSI	biogenic particulate silica	mol L^{-1}
C11	CFC11	mol L^{-1}
C14B	no-bomb 14C	mol L^{-1}
CAL	sinking $CaCO_3$	mol L^{-1}
CCH	chlorophyll in calcifiers	g L^{-1}
CFE	Fe in calcifiers	mol L^{-1}
CH4	methane	mol L^{-1}
COC	calcifying phytoplankton	mol L^{-1}
DCH	chlorophyll in silicifiers	g L^{-1}
DFE	Fe in silicifiers	mol L^{-1}
DIA	silicifying phytoplankton	mol L^{-1}
DIC	dissolved inorganic carbon	mol L^{-1}
DOC	dissolved organic carbon	mol L^{-1}
DMS	dimethylsulphide	mol L^{-1}
DMD	dimethylsulphoniopropionate	mol L^{-1}
DSI	sinking particulate silica	mol L^{-1}
FCH	chlorophyll in N_2 fixers	g L^{-1}
FER	dissolved iron	mol L^{-1}
FFE	Fe in N_2 fixers	mol L^{-1}
FIX	N_2 fixing phytoplankton	mol L^{-1}
FOR	foraminifers	mol L^{-1}
GEL	jellyfish / gelatinous zooplankton	mol L^{-1}
GOC	large particulate organic carbon	mol L^{-1}
GON	large particulate organic nitrogen	mol L^{-1}
HCH	chlorophyll in DMSP producers	mol L^{-1}
HFE	Fe in DMSP producers	mol L^{-1}
MAC	(crustacean) macrozooplankton	mol L^{-1}
MES	mesozooplankton	mol L^{-1}
MIX	mixed phytoplankton	mol L^{-1}
N2O	prognostic nitrous oxide	mol L^{-1}
N2S	diagnostic nitrous oxide	mol L^{-1}
NCH	chlorophyll in mixed phytoplankton	g L^{-1}
NFE	Fe in mixed phytoplankton	mol L^{-1}
NH4	ammonium + ammonia	mol L^{-1}
NO3	nitrate	mol L^{-1}
OXY	dissolved oxygen	mol L^{-1}
PCH	chlorophyll in pico-phytoplankton	g L^{-1}
PFE	Fe in pico-phytoplankton	mol L^{-1}
PIC	pico-phytoplankton	mol L^{-1}
PHA	DMSp producing phytoplankton	mol L^{-1}
PIIC	pre-industrial DIC	mol L^{-1}
PO4	phosphate	mol C L^{-1}
POC	small particulate organic carbon	mol L^{-1}
PRO	proto-zooplankton	mol L^{-1}
PTE	pteropods	mol L^{-1}
SFE	Fe in small POM	mol L^{-1}
SIL	dissolved SiO_3	mol L^{-1}

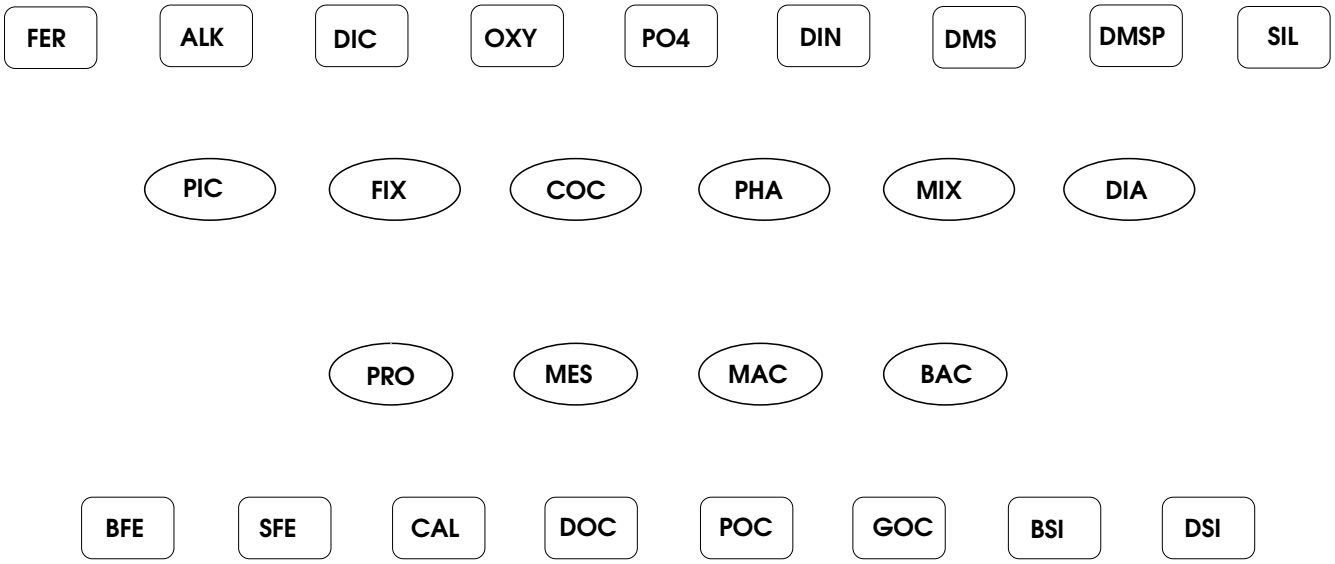

Figure 1: The constituents of PlankTOM; PFTs are shown as ellipses and tracers as rounded rectangles.There are also tracers for the chlorophyll and iron content of the individual pPFTs but these have been omitted from the figures for clarity.

2 Autotrophs

2.1 Primary Production, Photosynthesis and Phytoplankton Biomass - PIC, FIX, COC, PHA, MIX, DIA

The processes governing evolution of phytoplankton biomass for each P_i is shown in Figure 2. Evolution in terms of carbon is described in this section; chlorophyll (Section 2.3) and iron in phytoplankton (Section 2.2) are modelled similarly. Growth of phytoplankton modifies dissolved organic carbon (Section 4.1), silica (Section 6.2), calcium carbonate (Section 5.1), phosphate, dissolved inorganic nitrogen (Section 6.3), alkalinity (Section 5.3) and oxygen (Section 6.4) in the ocean.

The temporal evolution of phytoplankton biomass is given in the equation below:

$$\frac{\partial P_i}{\partial t} = \underbrace{\mu^{P_i} P_i}_{production} - \underbrace{\mu^{P_i} \delta^{P_i} P_i}_{loss} - \underbrace{\sum_j g_{P_i}^{Z_j} Z_j P_i}_{grazing} \tag{2}$$

$g_{P_i}^{Z_j} * Z_j * P_i$ describes the amount of biomass lost in grazing by the zPFT $Z_j, j \in \{1, 5\}$ as described in Section 3. In the present configuration of the model all available phytoplankton are grazed so there is no mortality term.

μ_P is the phytoplankton growth rate and is a function of temperature, light and nutrient availability:

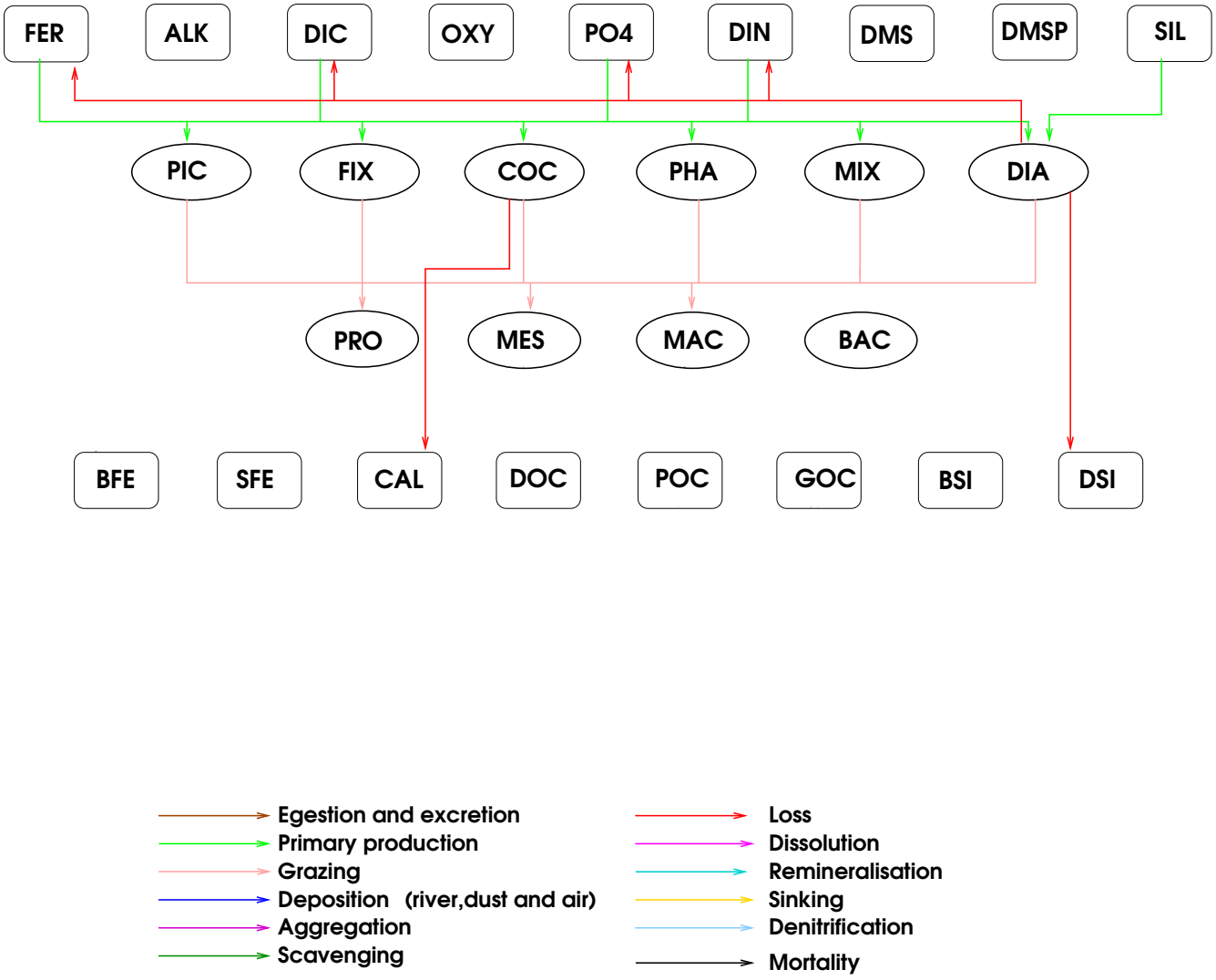

Figure 2: The processes governing the development of the phytoplankton.

$$\begin{aligned}\mu^{P_i} &= \mu_{opt}^{P_i} * (1 + \delta^{P_i}) * f(T) * f(PAR) * f(nut) \\ &= \mu_{opt}^{P_i} * (1 + \delta^{P_i}) * f(T) * L_{light}^{P_i} * L_{nut}^{P_i} \end{aligned} \tag{3}$$

where $\mu_{opt}^{P_i}$ is the optimum growth rate, and δ^{P_i} is the fraction of particulate photosynthesis that is respired.

The temperature dependence of the growth rate is

$$f(T) = e^{-1 * \frac{(T - Topt)^2}{\Delta T^2}} \tag{4}$$

where T_{opt} is the optimum temperature, at which $\mu = \mu_{opt}$, ΔT is the width of the temperature response, such that $\mu = \frac{\mu_{opt}}{e}$ at $T = T_{opt} \pm \Delta T$, and T is the seawater temperature in °Celsius.

For coccolithophorids the growth rate below 10° is reduced to $(0.2 + 0.8 * \frac{T}{10.}) * f(T)$.

The radiation available for photosynthesis is dependent on the wavelength and the depth:

$$\begin{aligned} PAR(z + \Delta z) &= .215 * Q_{sr} * e^{-\left(\sum_i x_g + CHL^{P_i} * y_g^{P_i}\right)\Delta z} \\ &+ .215 * Q_{sr} * e^{-\left(\sum_i x_r + CHL^{P_i} * y_r^{P_i}\right)\Delta z}. \end{aligned} \tag{5}$$

where the fraction of available solar radiation Q_{sr} which is in the photosynthetically active wavelength range has been divided between the blue/green and red wavelengths, x_g, x_r are the extinction coefficients of pure water for blue/green and red wavelengths and $y_g^{P_i}$, $y_r^{P_i}$ are the extinction coefficients of chlorophyll.

$$perfrm = \alpha^{P_i} * \frac{CHL^{P_i}}{P_i} 4.6 * PAR(z) \tag{6}$$

and

$$pctnut = \mu_0^{P_i} * (1 + \delta^{P_i}) * f(T) * L_{nut}^{P_i} \tag{7}$$

then

$$L_{light} = 1 - e^{-\frac{perfrm}{pctnut}} \tag{8}$$

The nutrient limitation ($L_{nut}^{P_i}$) determines the limitation of the growth rate due to the availability of nutrients. It is assumed that nutrient limitation follows Michaelis-Menten kinetics and that growth is determined by the least available nutrient. Hence, for phytoplankton other than silicifiers and nitrogen fixers:

Hence, for phytoplankton other than silicifiers and nitrogen fixers:

$$L_{nut}^{P_i} = \min\left(\frac{PO_4}{PO_4 + K_{PO_4}^{P_i}}, \frac{\frac{Fe_{P_i}}{P_i} - Fe_{P_i}^{min}}{Fe_{P_i}^{opt} - Fe_{P_i}^{min}}, dinlim\right) \tag{9}$$

$$dinlim = \frac{NH_4}{NH_4 + K_{NH4}^{P_i}} + \frac{NO_3(1 - \frac{NH_4}{NH_4 + K_{NH4}^{P_i}})}{NO_3 + K_{NO3}^{P_i}} \tag{10}$$

for silicifiers:

$$L_{nut}^{DIA} = \min\left(\frac{PO_4}{PO_4 + K_{PO_4}^{DIA}}, \frac{\frac{Fe_{DIA}}{DIA} - Fe_{DIA}^{min}}{Fe_{DIA}^{opt} - Fe_{DIA}^{min}}, dinlim, \frac{Si}{Si + K_{Si}^{DIA}}\right). \tag{11}$$

and for nitrogen fixers:

$$L_{nut}^{FIX} = \min\left(\frac{PO_4}{PO_4 + K_{PO_4}^{FIX}}, \frac{\frac{Fe_{FIX}}{FIX} - Fe_{FIX}^{min}}{Fe_{FIX}^{opt} - Fe_{FIX}^{min}}, dinlim + R_{FIX}\,(1 - dinlim)\right) \tag{12}$$

R_{fix} is the fraction of the maximum growth rate that can be achieved when growing on N_2.

2.2 Iron in phytoplankton / Fe in pPFTs - DFe, NFe, CFe, PFe, HFe, FFe

The iron content of phytoplankton (DFE for silicifiers, NFE for mixed-phytoplankton, CFE for calcifiers, PFE for picophytoplankton, HFE for DMS producers and FFE for N_2-fixers) is given by:

The iron content of phytoplankton (DFE for silicifiers, NFE for mixed-phytoplankton, CFE for calcifiers, PFE for picophytoplankton, HFE for DMS producers and FFE for N_2-fixers) is given by:

$$\begin{aligned}\frac{\partial Fe^{P_i}}{\partial t} &= \underbrace{\mu_{opt}^{P_i}(1+\delta^{P_i})f(T)L_{Q_{Fe}}^{P_i}L_{nutFe}^{P_i}P_i}_{production} - \underbrace{\mu_{opt}^{P_i}\delta_{P_i}f(T)L_{Q_{Fe}}^{P_i}L_{nutFe}^{P_i}P_i}_{loss} \\ &- \underbrace{\sum_j g_{P_i}^{Z_j}Z_j * Fe^{P_i}}_{grazing}\end{aligned} \tag{13}$$

$\rho_{Fe}^{P_i}$ describes the iron-light colimitation to phytoplankton growth [Buitenhuis and Geider, 2010] and is given by:

$$L_{Q_{Fe}}^{P_i} = \left(\frac{(\frac{\rho max}{\rho min} Fe_{P_i}^{max} - Fe_{P_i}^{max})(Fe_{Pi}^{max} - \frac{Fe_{P_i}}{P_i})}{(Fe_{P_i}^{max} - Fe_{P_i}^{min})} + Fe_{P_i}^{max} \right) * L_{light} \quad (14)$$

in which L_{light} is described in Eq. 8. For phytoplankton other than nitrogen fixers and silicifiers the nutrient limitation is given by:

$$L_{nutFe}^{P_i} = \min \left(\frac{PO_4}{PO_4 + K_{PO_4}^{P_i}}, \frac{FER}{FER + K_{FER}^{P_I}}, dinlim \right) \quad (15)$$

in which dinlim is defined in Eq. 10, for silicifiers

$$L_{nutFe}^{DIA} = \min \left(\frac{PO_4}{PO_4 + K_{PO_4}^{DIA}}, \frac{FER}{FER + K_{FER}^{DIA}}, dinlim, \frac{Si}{Si + K_{Si}^{DIA}} \right). \quad (16)$$

and for nitrogen fixers:

$$L_{nutFe}^{FIX} = \min \left(\frac{PO_4}{PO_4 + K_{PO_4}^{FIX}}, \frac{FER}{FER + K_{FER}^{FIX}}, dinlim + R_{FIX}\,(1 - dinlim) \right) \quad (17)$$

2.3 Chlorophyll - DCH, NCH, CCH, PCH, HCH, FCH

The chlorophyll content of each phytoplankton type (DCH for silicifiers, NCH for mixed-phytopla -nkton, CCH for calcifiers and PCH for picophytoplankton, HCH for DMS-producers and FCH for N_2-fixers) is modelled. Chlorophyll evolves in a very similar fashion to phytoplanktonic biomass (see equation 2), as sources and sinks of chlorophyll are of phytoplanktonic origin. The iron-light colimitation model is a dynamical photosynthesis model in which the rate of photosynthesis both controls cellular iron and chlorophyll synthesis and is controlled by their quota [Buitenhuis and Geider, 2010].

$$\begin{aligned} \frac{\partial Chl^{P_i}}{\partial t} &= \underbrace{\rho_{Chl}^{P_i} L_{light} pctnut P_i}_{production} - \underbrace{\mu_0^{P_i} \delta_{P_i} b_{P_i}^T * Chl^{P_i}}_{loss} \\ &- \underbrace{\sum_j g_{P_i}^{Z_j} Z_j \frac{Chl_{P_i}}{P_i}}_{grazing}, \end{aligned} \quad (18)$$

where

$$\rho_{Chl}^{P_i} = \theta_{chl}^{P_i} * pctnut * \frac{L_{light}}{perfrm} \quad (19)$$

$\theta_{chl}^{P_i}$ is the maximum chlorpophyll to carbon ratio for phytoplankton P_i and $perfrm$ and $pctnut$ are defined in equations 6 and 7

Table 2: List of Parameters and variables used to compute the evolution of phytoplankton

Term	**Variable**	**Description**	**Defined in**
δ_{P_i}	rn_resphy	respiration as fraction of growth	namelist.trc.sms
$\mu_{opt}^{P_i}$	rn_mumpft	optimum growth rate	namelist.trc.sms
$\mu^{P_i} P_i$	prophy	productivity of phytoplankton P_i	bgcpro.F90
T_{opt}	rn_mutpft	optimum temperature of growth rate	namelist.trc.sms
ΔT	rn_mudpft	width of temperature response curve	namelist.trc.sms
$f(T)$	tgfunc	temperature dependence of growth rate	bgcpro.F90
α^{P_i}	rn_alpphy	initial slope of photosynthesis vs light intensity curve	namelist.trc.sms
PAR	etot	Photosynthetcally active radiation	bgcpro.F90
Q_{sr}	qsr	surface solar radiation	traqsr.F90
x_g	rn_ekwgrn	absorption coefficient of water for blue-green light	namelist.trc.sms
x_r	rn_ekwred	absorption coefficient of water for red light	namelist.trc.sms
$y_g^{P_i}$	rn_kgrphy	absorption coefficient of chlorophyll for blue-green	namelist.trc.sms
$y_r^{P_i}$	rn_krdphy	absorption coefficient of chlorophyll for red light	namelist.trc.sms
$perfrm$	perfrm	photosynthetic performance	bgcpro.F90
$pctnut$	pctnut	macronutrient and temperature defined growth rate	bgcpro.F90
L_{light}	xlim8	Light limitation for phytoplankton growth	bgcpro.F90
$Fe_{P_i}^{max}$	rn_qmaphy	Maximum Fe quota	namelist.trc.sms
$Fe_{P_i}^{min}$	rn_qmiphy	Minimum Fe quota	namelist.trc.sms
$Fe_{P_i}^{opt}$	rn_qopphy	Optimum Fe quota	namelist.trc.sms
$K_{FER}^{P_i}$	rn_kmfphy	half saturation constant of Fe	namelist.trc.sms
$K_{NH4}^{P_i}$	rn_kmhphy	half-saturation coefficients for $NH4$	namelist.trc.sms
$K_{NO3}^{P_i}$	rn_kmnphy	half-saturation coefficients for $NO3$	namelist.trc.sms
$K_{PO4}^{P_i}$	rn_kmpphy	half-saturation coefficients for $PO4$	namelist.trc.sms
K_{SIL}^{DIA}	rn_sildia	half-saturation coefficient for SIL in diatoms	namelist.trc.sms
$L_{nut}^{P_i}$	xlimpft	macronutrient limitation for phytoplankton growth	bgcpro.F90
$\frac{\rho max}{\rho min}$	rn_rhfphy	ratio between iron starved and iron saturated maximum iron uptake rates	namelist.trc.sms
$\theta_{Chl}^{P_i}$	rn_thmphy	maximum CHL:C ratio	namelist.trc.sms
$\rho_{Chl}^{P_i}$	rhochl	regulation term of chlorophyll synthesis	bgcpro.F90

3 Heterotrophic PFT's

The temporal evolution of zooplankton and the pico-heterotrophs are shown in Figure 3.

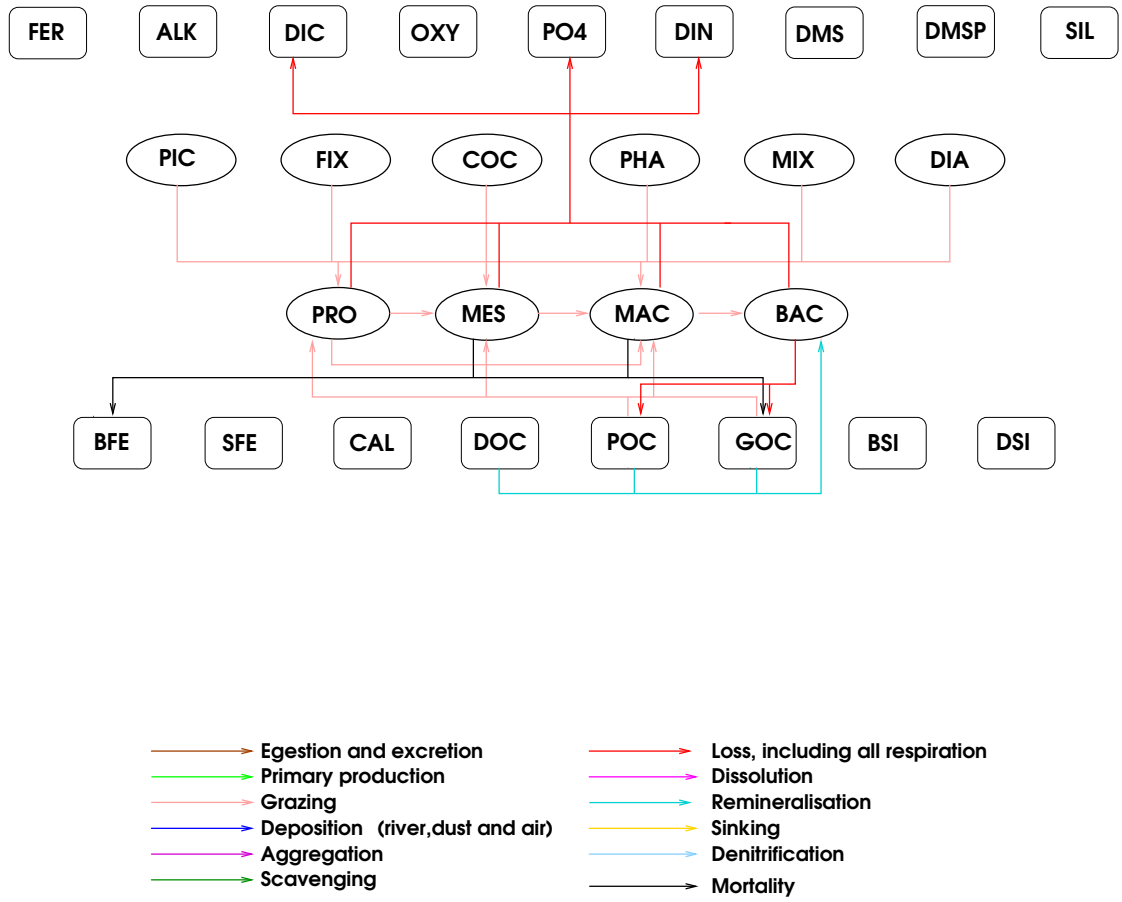

Figure 3: The processes governing the development of the zooplankton and pico-heterortrophs.

3.1 Zooplankton Biomass

The temporal evolution of zooplankton concentrations Z_j in PlankTOM are described as follows [Buitenhuis et al., 2006]:

$$\frac{\partial Z_j}{\partial t} = \underbrace{\sum_{k=1}^{j} g_{F_k}^{Z_j} * F_k * MGE * Z_j}_{growth\ through\ grazing} - \underbrace{\sum_{k=j}^{5} g_{Z_j}^{Z_k} * Z_j * Z_k}_{loss\ through\ grazing} - \underbrace{R_{0^\circ}^{Z_j} * d_{Z_j}^{T} * Z_j}_{basal\ respiration}$$
$$- \underbrace{m_{0^\circ}^{Z_j} * c_{Z_j}^{T} * \frac{Z_j}{K^{Z_j} + Z_j} * \sum_i (Z_j + P_i)}_{mortality\ through\ predation}, \quad (20)$$

where $g_{F_k}^{Z_j}$ is the grazing of zooplankton Z_j on food source F_k and MGE is the growth efficiency. $R_{0^\circ}^{Z_j}$ is the respiration rate at 0°C, d_{Z_j} is the temperature dependence of the respiration ($d^{10} = Q_{10}$). $m_{0^\circ}^{Z_j}$ is the mortality rate at 0°C, c_{Z_j} is the temperature dependence of the mortality ($c^{10} = Q_{10}$). K^{Z_j} is the half saturation constant for mortality and is set to $20 * 10^{-6}$.

The mortality term for jellyfish and macrozooplankton is due to predation by top predators for which the total zooplankton plus phytoplankton biomass is used as a proxy.

In the presence of ice krill are protected from predation so the macrozooplankton mortality is reduced by a factor of .01.

Grazing $g_{F_k}^{Z_j}$, of zooplankton Z_j on food source F_k is dependent on the zooplankton preference, $p_{F_k}^{Z_j}$, the concentration of the food source and the temperature

$$g_{F_k}^{Z_j} = f(T) \frac{p_{F_k}^{Z_j}}{K^{Z_j} + \sum_i p_{F_k}^{Z_j} F_k} \quad (21)$$

in which f(T) is defined in Eq. 4. The food sources F for zooplankton are shown in Table 3.

Table 3: Food sources for zooplankton and pico-heterotrophs

Z_j / Food	Macro-	Jellyfish	Meso-	Pteropods	Proto-zooplankton	Pico-heterotrophs
Macro-zooplankton		*				
Jellyfish	*					
Meso-zooplankton	*	*				
Pteropods	*	*	*			
Proto-zooplankton	*	*	*	*		
Phytoplankton	*	*	*	*	*	
Pico-heterotrophs	*	*	*	*	*	
Large POM	*	*	*	*	*	*
Small POM	*	*	*	*	*	*
Dissolved OM						*

In shallow water (<600m) in the summer months under ice coverage of between .1 and .3 macrozooplankton experience enhanced recruitment [Wiedenmann et al., 2009]. This is included by increasing the growth rate by a factor r_{MAC} when these conditions apply.

The model growth efficiency MGE, a function of gross growth efficiency (GGE), describes the fraction of grazed food incorporated into zooplankton biomass and basal respiration normalised to all material ingested. Equation 39 shows the possible reduction in MGE_{Z_j} when zooplankton graze on phytoplankton with a lower $\frac{Fe}{C}$ ratio than themselves.

Table 4: List of parameters and variables used to calculate the evolution of zooplankton

Term	**Variable**	**Description**	**Defined in**
$g_0^{Z_j}$	rn_grazoo	zooplankton optimum grazing rate	namelist.trc.sms
$g_{max}^{Z_j}$	graze	grazing rate at local T	bgclos.F90
b_{Z_j}	rn_mutpft	Temperature dependence of grazing	namelist.trc.sms
r_{MAC}	rn_icemac	enhanced recruitment factor under ice	namelist.trc.sms
p_F^Z	rn_prfzoo	zooplankton grazing preferences	namelist.trc.sms
K^{Z_j}	rn_grkzoo	half-saturation constant for grazing	namelist.trc.sms
σ^{Z_j}	rn_sigzoo	Fraction of zooplankton excretion as DIC	namelist.trc.sms
ξ^{Z_j}	rn_unazoo	Fraction of unassimilated food	namelist.trc.sms
MGE_{Z_j}	mgezoo	model growth of efficiency	bgcbio.F90
$R_{0^\circ}^{Z_j}$	rn_reszoo	zooplankton respiration at 0°C of	namelist.trc.sms
d_{Z_j}	rn_retzoo	Temperature dependence of zoo. respiration	namelist.trc.sms
$m_{0^\circ}^Z$	rn_mormac	mortality at 0°C of macrozoo.	namelist.trc.sms
c_{Z_j}	rn_motmac	temperature dependence of mortality	namelist.trc.sms
GGE_{Z_j}	rn_ggezoo	Growth efficiency	namelist.trc.sms

3.2 Pico-heterotrophs

The temporal evolution of bacterial concentration is modelled in a similar way to zooplankton:

$$\begin{aligned}\frac{\partial BAC}{\partial t} &= \underbrace{\sum \lambda_{OC}^{*} BGE * BAC}_{growth\ through\ remineralisation} - \underbrace{R_{0^\circ}^{BAC} * d_{BAC}^{T} * BAC}_{respiration} \\ &- \underbrace{\sum_j g_{BAC}^{Z_j} * BAC * Z_j}_{grazing} \end{aligned} \tag{22}$$

where BGE is the bacterial growth efficiency.

The food sources OM for bacteria are DOC, small and large particulate organic carbon and iron (POC, GOC, SFe and BFe).

Mineralisation rate λ^*_{OM} is dependent on the temperature and the available food:

$$\lambda^*_{OM} = M_{opt} f(T) \eta_O \frac{\sum_k p^{BAC}_{OC} OM}{K^{BAC}_{OC} + \sum_k p^{BAC}_{OC} OC}, \tag{23}$$

where M_{opt} is the optimum assimilation rate, f(T) is defined in Eq. 4, bacterial growth is dependent on the available oxygen:

$$\eta_O = \frac{OXY + 3 * 10^{-6}}{OXY + 10 * 10^{-6}}, \tag{24}$$

which leads to a maximum bacterial growth rate in the absence of oxygen that is 0.3 times the maximum growth rate at high oxygen, each food source is associated with a preference p^{BAC}_{OC}, OM in the numerator can be either carbon or iron, while OC in the denominator is always carbon.

K^{BAC}_{OC} is the half-saturation constant for mineralisation of organic matter.

$R^{BAC}_{0^\circ}$ is the respiration rate at 0°C, d_{BAC} is the temperature dependence of the respiration ($d^{10} = Q_{10}$).

Bacterial growth efficiency BGE, which describes the fraction of mineralised food incorporated into bacterial biomass, is a function temperature and iron availability :

$$BGE = min(BGE_{0^\circ} - e * T, \frac{FER_{BAC} + \lambda^*_{SFe} BAC + \lambda^*_{BFe} BAC)}{max((\lambda^*_{DOC} BAC + \lambda^*_{POC} BAC + \lambda^*_{GOC} BAC) * \frac{Fe}{C}_H, 1e-25)}) \tag{25}$$

where BGE_{0° is the bacterial growth efficiency at 0° and e is the temperature dependence of bacteria growth, FER_{BAC} is the uptake of dissolved Fe (see equation 48), and $\lambda^*_{GOC}, \lambda^*_{DOC}, \lambda^*_{POC}$ are the remineralisation rates for DOC, GOC and POC respectively as defined above.

Grazing of bacteria by zooplankton is described in the previous section.

3.2.1 Denitrification

When waters become suboxic, bacteria can also use nitrate in order to gain oxidative power for DOC remineralization. Hence, there is a (bacterial) denitrification term in the model (Eq. 62).

Table 5: List of parameters and variables used to calculate the evolution of pico-heterotrophs

Term	**Variable**	**Description**	**Defined in**
M_{opt}	rn_grabac	Optimum assimilation rate of bacteria	namelist.trc.sms
K_{OC}^{BAC}	rn_kmobac	carbon half saturation constant of bacteria	namelist.trc.sms
p_F^{BAC}	rn_gbadoc	bacterial preference for DOC	namelist.trc.sms
	rn_gbapoc	bacterial preference for POC	namelist.trc.sms
	rn_gbagoc	bacterial preference for GOC	namelist.trc.sms
	rn_gbagon	bacterial preference for GON	namelist.trc.sms
BGE_{0°	rn_ggebac	Bacterial growth efficiency at 0°	namelist.trc.sms
$R_{0^\circ}^{BAC}$	rn_resbac	respiration at 0°C	namelist.trc.sms
d_{BAC}	rn_retbac	Temperature dependence of respiration	namelist.trc.sms
e	rn_ggtbac	Temperature dependence of bacterial growth efficiency	namelist.trc.sms
FER_{BAC}	ubafer	Uptake of dissolved Fe by bacteria	bgcsnk.F90
η_O	$\frac{OXY+3*10^{-6}}{OXY+10*10^{-6}}$	oxygen limitation to bacteria growth	
$\lambda^*_{SFe}BAC$	remsfe	remineralisation of Fe in POC	bgcsnk.F90
$\lambda^*_{BFe}BAC$	rembfe	remineralisation of Fe in GOC	bgcsnk.F90
$\lambda^\star_{DOC}BAC$	remdoc	remineralisation of DOC	bgcnul.F90,bgcsnk.F90
$\lambda^\star_{POC}BAC$	rempoc	remineralisation of POC	bgcnul.F90,bgcsnk.F90
$\lambda^\star_{GOC}BAC$	remgoc	remineralisation of GOC	bgcnul.F90,bgcsnk.F90
$\frac{Fe}{C}_H$	ferat3	Fe:C of heterotrophs	trcini_planktom.F90

4 Organic matter and bacterial Remineralisation

The source and sinks for dissolved organic carbon (DOC) and small (POC) and large (GOC) particulate carbon are shown in Figure 4.

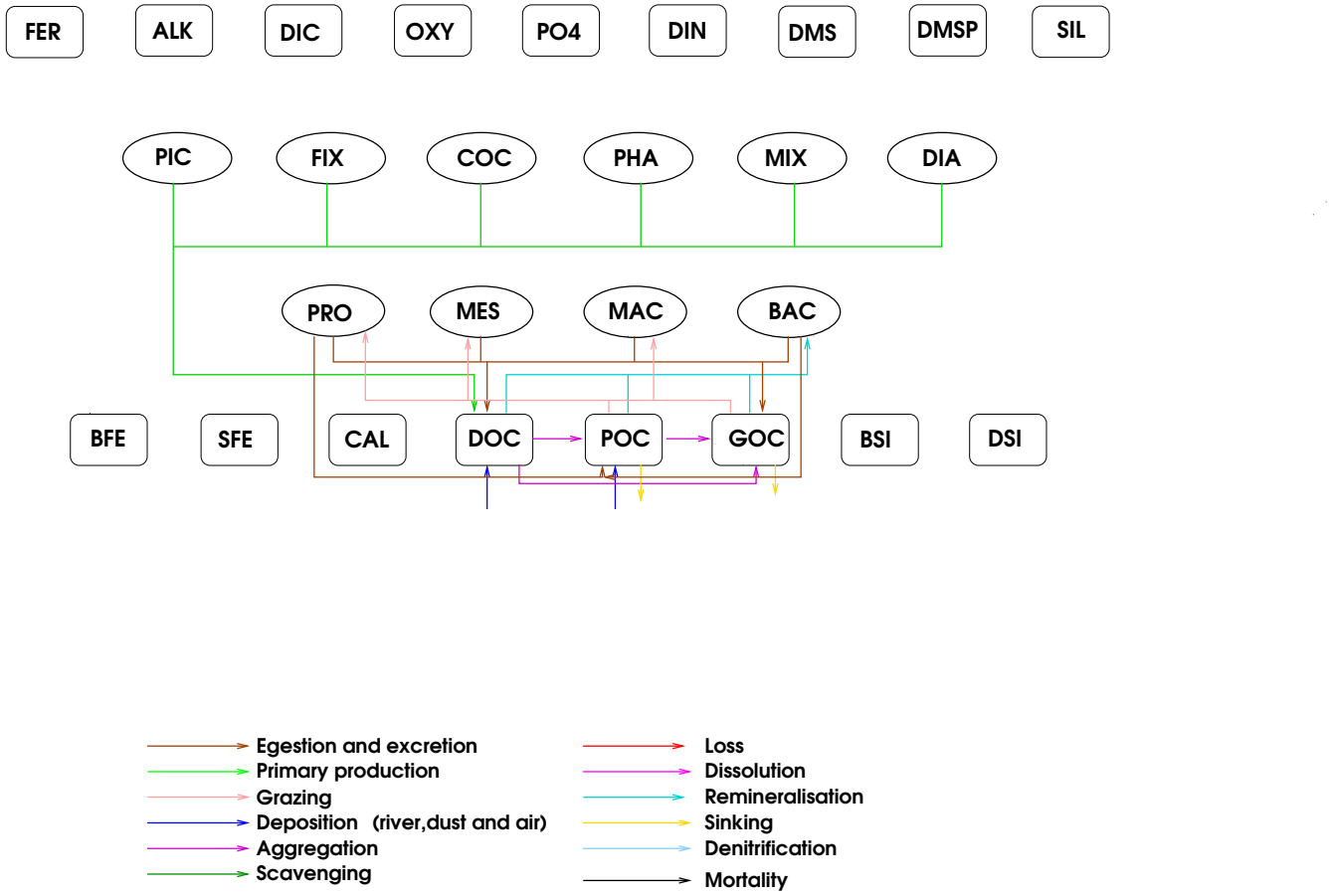

Figure 4: The source and sinks for dissolved organic carbon (DOC) and small (POC) and large (GOC) particulate carbon.

4.1 Dissolved Organic Carbon - DOC

The evolution of DOC is calculated in the following way:

$$\begin{aligned}\frac{\partial DOC}{\partial t} &= \underbrace{\sum \nu_{P_i}^{tot} \mu^{P_i} P_i}_{production} + \underbrace{\sum_j \left[(1-\sigma^{Z_j})(1-\xi^{Z_j} - MGE^{Z_j}) \sum_k g_{F_k}^{Z_j} * F_k * Z_j \right]}_{egestion} \\ &+ \underbrace{.333 R_{0^\circ}^{BAC} d_{BAC}^T BAC}_{excretion} - \underbrace{\lambda_{DOC}^\star BAC}_{remineralisation} - \underbrace{\Phi_{agg}^{DOC \to POC} - \Phi_{agg}^{DOC \to GOC}}_{aggregation} \\ &+ \underbrace{DOC_{riv}}_{river\ input}, \end{aligned} \tag{26}$$

where $\nu_{P_i}^{tot} = \nu_{P_i} + (1 - L_{nut}^{P_i}) \nu_{P_i}^{max}$ is the fraction of phytoplankton growth (Eq. 3) which forms DOC. Bacterial degradation of DOC is given by equation 23.

The aggregation functions $\Phi_{agg}^{X \to Y}$ are described in Section 4.2.

Table 6: List of Parameters used in bacterial remineralisation of DOC

Term	Variable	Description	Defined in
ν_{P_i}	rn_docphy	minimum DOC excretion ratio	namelist.trc.sms
$\nu_{p_i}^{max}$	rn_domphy	maximum DOC excretion ratio	namelist.trc.sms
$g_{F_i}^{Z_j} Z_j$	grazoc	Total grazing by zPFT	bgclos.F90
d_{BAC}	rn_retbac	temperature dependence of bacterial respiration	namelist.trc.sms
DOC_{riv}	depdoc	River input of DOC	trcini

4.2 Particulate aggregation

Particle aggregation through either differential sinking or turbulent coagulation is calculated by:

$$\begin{aligned}\Phi_{agg}^{DOC \to POC} &= \phi_5^{DOC} \epsilon DOC^2 + \phi_7^{DOC} \epsilon DOC\, POC \\ \Phi_{agg}^{DOC \to GOC} &= \phi_6^{DOC} \epsilon\, DOC\, GOC \\ \Phi_{agg}^{POC \to GOC} &= \phi_1^{POC} \epsilon POC^2 + \phi_2^{POC} \epsilon GOC\, POC \\ &\quad + \phi_3^{POC} POC\, GOC + \phi_4^{POC} POC^2 \end{aligned} \tag{27}$$

In which ϵ is the shear rate. The coefficients ϕ were obtained by integrating the standard curvilinear kernels for collisions over the size range of each organic matter pool.

Table 7: List of Parameters used in particulate aggregation

Term	Variable	Description	Defined in
$\Phi_{agg}^{DOC \rightarrow POC}$	xaggdoc	DOC-POC aggregation	bgcsnk.F90
$\Phi_{agg}^{DOC \rightarrow GOC}$	xaggdoc2	DOC-GOC aggregation	bgcsnk.F90
$\Phi_{agg}^{POC \rightarrow GOC}$	xagg	POC-GOC aggregation	bgcsnk.F90
ϕ_5^{DOC}	rn_ag5doc	DOC-POC aggregation	namelist.trc.sms
ϕ_7^{DOC}	rn_ag7doc	DOC-POC aggregation	namelist.trc.sms
ϕ_6^{DOC}	rn_ag6doc	DOC-GOC aggregation	namelist.trc.sms
ϕ_1^{POC}	rn_ag1poc	POC-GOC aggregation	namelist.trc.sms
ϕ_2^{POC}	rn_ag2poc	POC-GOC aggregation	namelist.trc.sms
ϕ_3^{POC}	rn_ag3poc	POC-GOC aggregation	namelist.trc.sms
ϕ_4^{POC}	rn_ag4poc	POC-GOC aggregation	namelist.trc.sms

4.3 Sinking

Using the data in Ploug et al. [2008] and applying the drag equations of Buitenhuis et al. [2001] results in a new function describing the relationship between particle density and sinking speed [Buitenhuis et al., 2013]:

$$V_{sink} = k_{GOC} * MAX(\rho_{particle} - \rho_{seawater}, \rho_{min})^{S_{GOC}}, \tag{28}$$

where, if ρ_{GOC} (=1.08), ρ_{CAL} (=1.34) and ρ_{DSI} (=1.2) are the densities of the organic matter, $CaCO_3$, and SiO_2 respectively, the particle density $\rho_{particle}$ is calculated by:

$$\rho_{particle} = \frac{(GOC * 240. + CAL * 100. + DSI * 60.)}{\max(\frac{GOC*240.}{\rho_{GOC}} + \frac{CAL*100.}{\rho_{CAL}} + \frac{DSI*60.}{\rho_{DSI}}, 10^{-15})} \tag{29}$$

and

$$\rho_{min} = \left(\frac{S_{POC}}{k_{GOC}}\right)^{\frac{1}{S_{GOC}}} \tag{30}$$

4.4 Sediment model

PlankTOM has a very simple sediment model in order to prevent the accumulation of very high particulate matter in the bottom water layer, which led to instabilities in the tracer advection. The sediment model is one layer below the bottom water layer. To facilitate computation, the height of the sediment is the same as the height of the bottom

Table 8: List of Parameters used in sinking

Term	Variable	Description	Defined in
S_{POC}	rn_snkpoc	sinking speed of POC	namelist.trc.sms
S_{GOC}	rn_snkgoc	sinking speed parameter for GOC	namelist.trc.sms
k_{GOC}	rn_singoc	second sinking speed parameter for GOC	namelist.trc.sms
ρ_{min}	dnsmin	density at which GOC sinking speed is rn_snkpoc	trcnam_planktom.F90
$\rho_{seawater}$	rhop	density of sea-water	
$\rho_{particle} - \rho_{seawater}$	xdens	density of particle	bgcsnk.F90
V_{sink}	xvsink	sinking speed of particle	bgcsnk.F90

water layer (fse3t), so that inventories and concentrations may be treated as interchangeable. The sediment layer receives material from sinking fluxes of POC, GOC, GON, CAL, ARA, DSI, SFE and BFE. The remineralisation rates are the same as in the overlying bottom water layer (equations 23, 35, 50). Nutrients are removed from the sediment model to balance river and dust inputs and thus maintain constant inventories.

4.5 Small particulate organic carbon - POC

The temporal evolution of small particulate organic carbon, POC, is calculated as

$$\begin{aligned}
\frac{\partial POC}{\partial t} = & \underbrace{\xi^{PRO} * \sum_{F_i} g_{F_i}^{PRO} PRO}_{proto-zooplankton\ unassimilated\ food} - \underbrace{\sum_{Z_j} g_{POC}^{Z_j} * Z_j * POC}_{grazing\ on\ POC} \\
& + \underbrace{0.333 * R_{0^\circ}^{BAC} * d_{BAC}^{T} * BAC}_{excretion} - \underbrace{\lambda_{POC}^{\star} BAC}_{POC\ remineralisation} - \underbrace{S_{POC} \frac{\partial POC}{\partial z}}_{POC\ sinking} \\
& + \underbrace{\Phi_{agg}^{DOC \to POC}}_{aggregation\ to\ POC} - \underbrace{\Phi_{agg}^{POC \to GOC}}_{aggregation\ to\ GOC} + \underbrace{POC_{riv}}_{river\ input} . \qquad (31)
\end{aligned}$$

Here, ξ^{PRO} is the unassimilated fraction of grazed material, $g_{F_i}^{PRO}$ are the grazing coefficients of proto-zooplankton on food sources F as specified in equation 20, and all others variables are as above.

Table 9: List of parameters and variables used to calculate the evolution of POC

Term	Variable	Description	Defined in
K_{P_i}	rn_snkpoc	sinking speed POC	namelist.trc.sms
POC_{riv}	deppoc	river input of POC	trcini

4.6 Large particulate organic carbon - GOC

The temporal derivative of large particulate organic carbon (GOC) is calculated as

$$\begin{aligned}\frac{\partial GOC}{\partial t} &= \underbrace{\sum_j \xi^{Z_j} \sum_k g_{F_k}^{Z_j} * Z_j * F_k}_{zooplankton\ unassimilated\ food} - \underbrace{\sum_j g_{GOC}^{Z_j} * Z_j * GOC}_{loss\ through\ grazing} + \underbrace{\sum_j m_{0^\circ}^{Z_j} * c^T * Z_j}_{MES,MAC\ mortality} \\ &+ \underbrace{\Phi_{agg}^{DOC\to GOC} + \Phi_{agg}^{POC\to GOC} PHA}_{aggregation\ to\ GOC} - \underbrace{\lambda_{GOC}^{\star} BAC}_{GOC remineralisation} - \underbrace{V_{sink} \frac{\partial GOC}{\partial z}}_{GOC sinking}. \end{aligned} \tag{32}$$

ξ^{Z_j} is unassimilated fraction of material grazed by meso- and macro-zooplankton and m^{Z_j} is meso- and macro-zooplankton mortality as in equation (20). V_{sink} is the sinking rate of GOC and is calculated as equation (28).

5 Carbonate chemistry

5.1 Calcite - CAL and Aragonite - ARA

Calcification in the model is performed by phytoplankton calcifiers, COC, pteropods, PTE, and, in PlankTOM12.0 only, foraminifers, FOR. The sources and sinks for detached $CaCO_3$ (CAL and ARA), dissolved inorganic carbon (DIC) and alkalinity (ALK) are shown in Figure 5

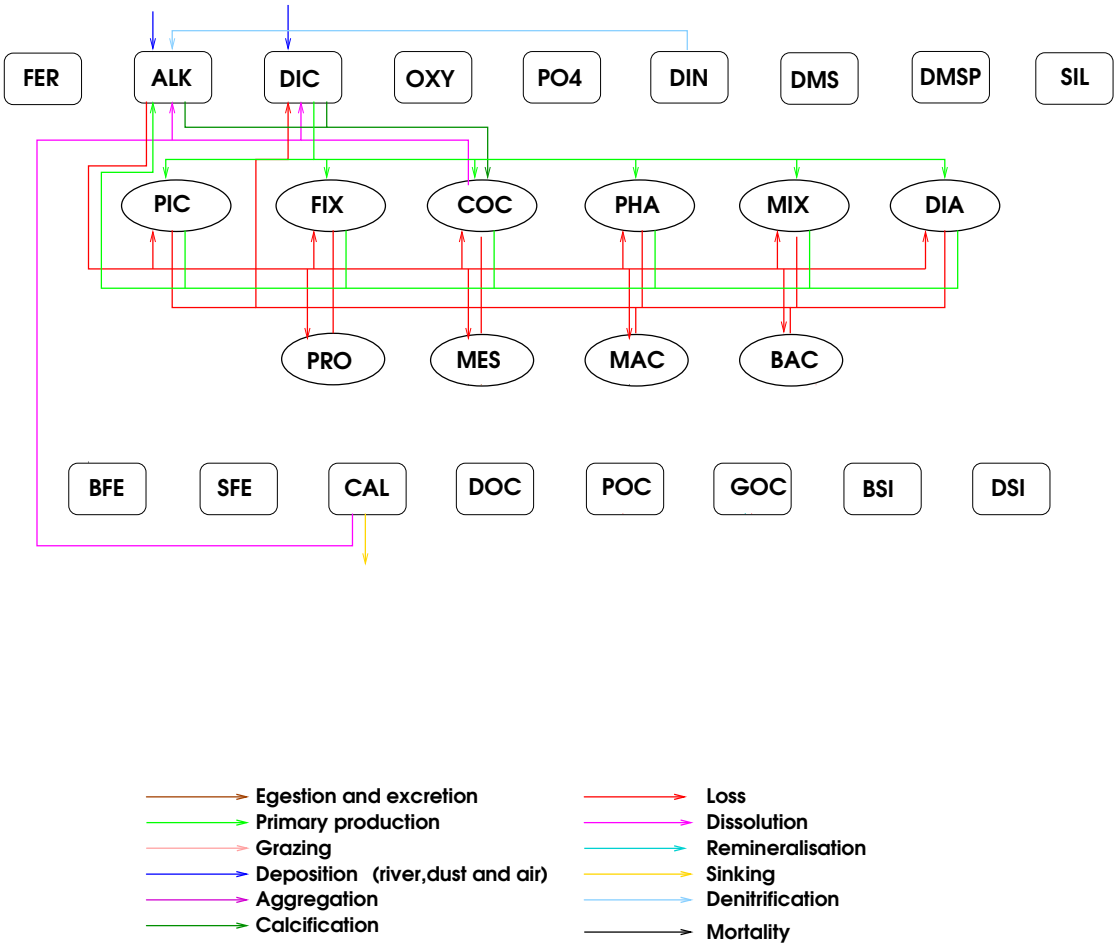

Figure 5: The source and sinks for detached carbonate (CAL), dissolved inorganic carbon (DIC) and alkalinity (ALK).

Attached $CaCO_3$ is produced in a fixed ratio to organic matter and therefore there are no tracers for their concentration. It does, however, reduce alkalinity, ALK, and dissolved inorganic carbon, DIC. Losses of calcifiers result in detached/sinking $CaCO_3$, and enters the tracer CAL (COC and FOR) or ARA (PTE).

$$\frac{\partial CaCO_{3attached}}{\partial t} = R_{CAL} \underbrace{\mu^{COC} COC}_{production\ by\ COC} \tag{33}$$

For detached $CaCO_3$, CAL and ARA:

$$\frac{\partial CAL}{\partial t} = R_{CAL}(1 - R_{diss}) \left(\underbrace{\mu_0^{COC} \delta_{COC} b_{COC}^T COC}_{COC\ loss} + \underbrace{\sum_j g_{COC}^{Z_j} Z_j * COC}_{grazing\ by\ zooplankton} \right) - \underbrace{V_{sink} \frac{\partial CAL}{\partial z}}_{sinking} - \underbrace{\beta_{CO_3} CAL}_{dissolution}, \tag{34}$$

where R_{CAL} is the calcification to calcifier organic carbon production ratio, R_{diss} is the fraction of attached $CaCO_3$ that is dissolved during losses of calcifiers, V_{sink} is the sinking speed of large particles and is described in section 4.3, and β_{CO_3} is the dissolution rate:

$$\beta_{CO_3} = MAX\left(M_{CO_3} * 1 - \Omega_{sat}, 0\right) \tag{35}$$

where Ω_{sat} is the deviation from saturation and M_{CO_3} is the maximum dissolution rate when Ω_{sat} = 0.

CAL and ARA are calculated in bgcbio.F90 and reduced by dissolution in bgclys.F90.

5.2 Dissolved inorganic carbon - DIC

The temporal evolution of dissolved inorganic carbon, DIC, is calculated as:

$$\frac{\partial DIC}{\partial t} = \underbrace{-\sum_i \mu^{P_i} * \left(1 + \nu_{P_i}^{TOT}\right) P_i}_{primary\ production} + \underbrace{consum}_{remineralisation} - \underbrace{R_{CAL} \mu^{COC} COC}_{attached\ CaCO_3} + R_{diss} R_{CAL} \left(\underbrace{\mu_0^{P_I} \delta_{COC} b_{COC}^T COC}_{COC\ loss} + \underbrace{\sum_j g_{COC}^{Z_j} Z_j COC}_{grazing\ by\ zooplankton} \right) + \underbrace{DIC_{riv}}_{river\ input} + \underbrace{\beta_{CO_3} CAL}_{dissolution} + \underbrace{F_{air-sea}^{CO_2}}_{air-sea\ flux}. \tag{36}$$

In addition to the inclusion of grazing by zooplankton remineralistion by bacteria is included as a function of

Table 10: List of parameters and variables used to calculate the evolution of calcite

Term	Variable	Description	Defined in
R_{CAL}	rn_coccal	$CaCO_3$:C_{org} ratio coccolithophores	namelist.trc.sms
	rn_forcal	$CaCO_3$:C_{org} ratio foraminifers	namelist.trc.sms
	rn_pteara	$CaCO_3$:C_{org} ratio pteropods	namelist.trc.sms
$\mu^{COC}COC$	prophy	coccolithophorid productivity	bgcpro.F90
	Eq. 20	PTE and FOR growth	bgclos.F90
R_{diss}	rn_discal	Fraction of $CaCO_3$ dissolved during coccolithophorid death	namelist.trc.sms
	rn_disfor	during foraminifer death	namelist.trc.sms
	rn_disara	during pteropod death	namelist.trc.sms
M_{CO_3}	rn_lyscal	maximum calcite dissolution rate	namelist.trc.sms
	rn_lysara	maximum aragonite dissolution rate	namelist.trc.sms
Ω_{sat}	omecal	calcite saturation state	bgclys.F90
	omeara	aragonite saturation state	bgclys.F90
$\beta_{CO_3}CAL$	remco3	calcite dissolution	bgclys.F90
	remara	aragonite dissolution	bgclys.F90
$V_{sink}CAL$	snkcal	sedimentation rate of calcite	bgcsnk.F90
	snkara	sedimentation rate of aragonite	bgcsnk.F90

their growth efficiency and respiration (in this case subscript j includes the pico-heterotrophs):

$$
\begin{aligned}
consum &= \underbrace{\sum_j \sigma^{Z_j} * (1 - \xi^{Z_j} - MGE^{Z_j}) \sum_k g_{F_k}^{Z_j} * Z_j * F_k}_{foodrespiration} \\
&+ \underbrace{(1 - BGE) * (\lambda^\star_{DOC} BAC + \lambda^\star_{POC} BAC + \lambda^\star_{GOC} BAC)}_{remineralisation} \\
&+ \underbrace{\sum_{j=1}^{3} R_{0^\circ}^{Z_j} d_{Z_j}^T Z_j}_{basal\ respiration} + \underbrace{.333 R_{0^\circ}^{BAC} d_{BAC}^T BAC}_{respiration} + \underbrace{\sum_i \delta_{P_i} b_{P_i}^T \mu_0^{P_i} P_i}_{loss} . \qquad (37)
\end{aligned}
$$

The bacterial growth efficiency, BGE, is given by Equation 25. The terms for attached $CaCO_3$ and production of DIC by dissolution are described in Section 5.1. River deposition DIC_{riv} is the input of DIC from rivers, see Section 8.6. The air-to-sea flux is described in section 7.

Dissolved inorganic carbon is calculated in bgcbio.F90; in bgclys.F90 the $CaCO_3$ dissolution to DIC is included while in bgcflx.F90 the air-sea flux of DIC is added.

Table 11: List of Parameters used in the evolution of DIC and ALK

Term	Variable	Description	Defined in
BGE	bactge	bacteria growth efficiency	bgcbio,bgcsnk.F90
DIC_{riv}	depdic	river input of DIC	river.nc, trcini
$R_{\frac{N}{C}}$	alknut	N+S+P to Carbon ratio	trcini

5.3 Alkalinity - ALK

The temporal evolution of alkalinity is calculated as:

$$\begin{aligned}\frac{\partial ALK}{\partial t} &= R_{\frac{N}{C}}\Big(\underbrace{\sum_i \mu^{P_i} P_i(1+\nu_{P_i}^{tot})}_{production} - \underbrace{consum}_{remineralisation}\Big) - \underbrace{2 * R_{CAL}\mu^{coc}COC}_{calcification} \\ &+ \underbrace{2R_{CAL}R_{diss}\big(\mu_0^{COC}\delta_{coc}b_{COC}^{T}COC + \sum_j g_{coc}^{Z_j}Z_jCOC\big)}_{dissolution} \\ &+ \underbrace{DIC_{riv}}_{river\ input} + \underbrace{N_{denit}}_{denitrification} + \underbrace{2 * \beta_{CO_3}CaCO_3}_{dissolution} \end{aligned} \quad (38)$$

where $R_{\frac{N}{C}} = \frac{N+S+P}{C} = \frac{16+6+1}{122}$ is the effect of nutrient uptake and remineralisation on alkalinity [Wolf-Gladrow et al., 2007]. The terms for the production of attached $CaCO_3$, dissolved COC and dissolved $CaCO_3$ are described in Section 5.1. River deposition, DIC_{riv} is described in Section 8.6 and denitrification, N_{denit} in Section 6.3.

6 Nutrients and gases

The processes governing the evolution of dissolved iron (FER), large (BFE) and small (SFE) particulate iron, dissolved silica (SIL), biogenic silica (BSI) and detrital silica (DSI) are shown in Figure 6.

The processes governing the evolution of phosphate (PO4), dissolved inorganic nitrogen (NO3 and NH4) and gases (OXY and optionally N2S, N2O and DMS) are shown in Figure 7.

6.1 The Iron Cycle

6.1.1 Fe in PFTs

The iron content of phytoplankton is presented in Section 2.2. The Fe/C ratio of zooplankton is fixed. If zooplankton graze on phytoplankton that have a higher Fe:C ratio than themselves, the excess is remineralised to dissolved

iron. If the phytoplankton Fe/C ratio is lower than zooplankton Fe:C, the model growth efficiency (MGE) is decreased:

$$MGE^{Z_j} = MIN\left(1-\xi^{Z_j}, GGE_{Z_j} + \frac{R_{0^\circ}^{Z_j} d_{Z_j}^T Z_j}{\sum_k g_{F_k}^{Z_j}}, \frac{\sum_k g_{F_k}^{Z_j} \frac{Fe_{F_k}}{F_k}(1-\xi^{Z_j})}{MAX\left(\sum_k g_{F_k}^{Z_j}\left(\frac{Fe}{C}\right)_Z, 1e-25\right)}\right) \quad (39)$$

6.1.2 Fe in detrital matter - BFE, SFE

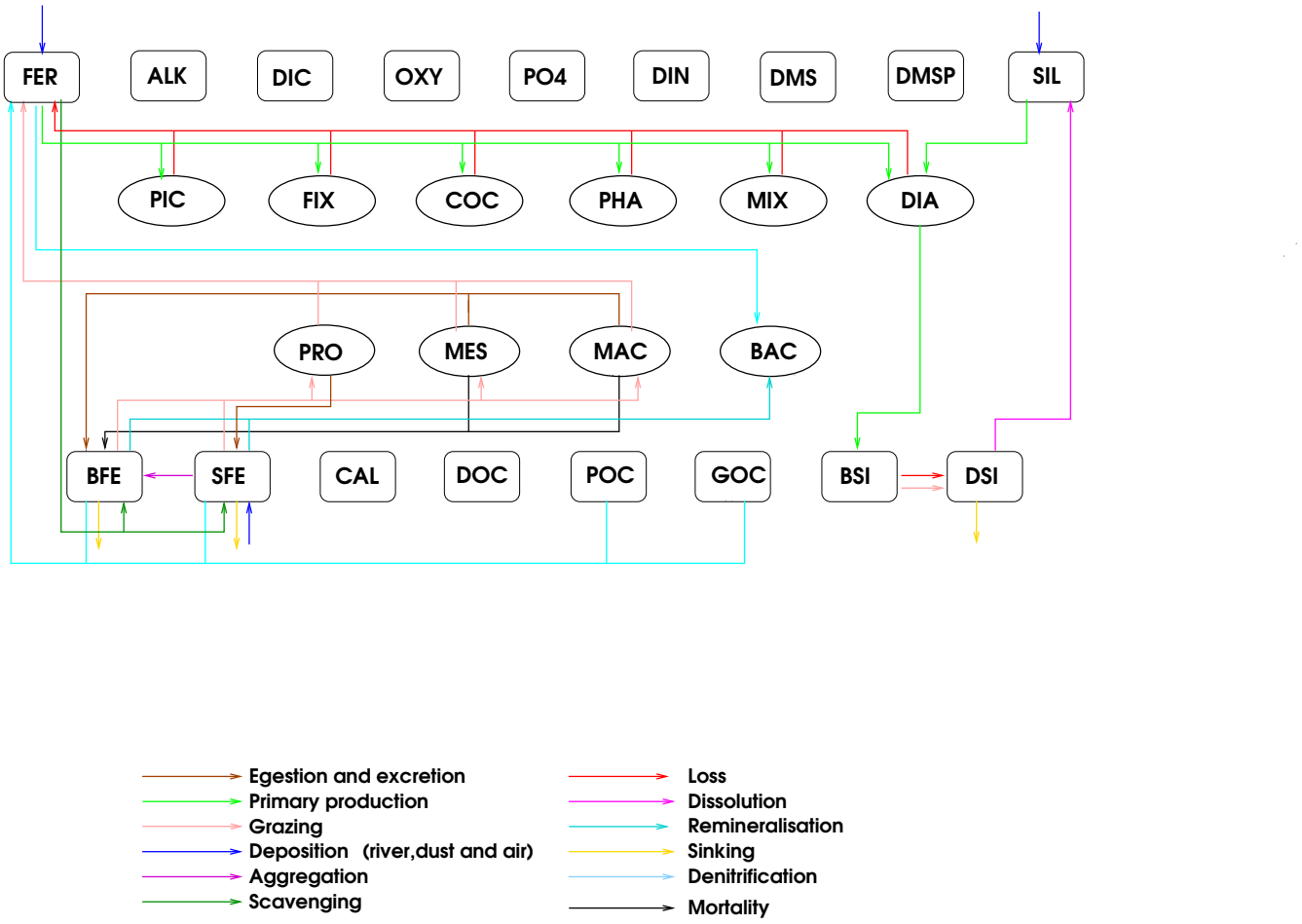

Figure 6: The sources and sinks for dissolved iron (FER), large (BFE) and small (SFE) particulate iron, dissolved silica (SIL), biogenic silica (BSI) and detrital silica (DSI).

Iron in detrital matter is divided into BFE in large organic particles (GOC) and SFE in small organic particles (POC). Production terms of particulate organic iron follow the Fe/C ratio of the source organisms. There is no iron

in DOM, but iron is added from dissolved iron to particulate organic iron during degradation of DOM. Degradation of POM conserves the Fe:C ratio of POM. The bottom correction removes as much carbon from the bottom water layers as is added by rivers (Section 8.6). Because iron is scavenged, the Fe/C ratio of POM sometimes becomes excessive. It is therefore set to a maximum, currently $2 * 10^{-6}$ mol:mol.

$$\begin{aligned}
\frac{\partial BFE}{\partial t} &= \underbrace{Fe_{scave}(POC + GOC + DSI + CAL)GOC}_{scavenging} - \underbrace{\sum_j g_{GOC}^{Z_j} * Z_j * GOC \frac{BFE}{GOC}}_{grazing\ loss} \\
&+ \underbrace{\left(\frac{Fe}{C}\right)_Z \sum_{j=MES,MAC} m_{0^\circ}^{Z_j} c^T z^j}_{mortality} + \underbrace{\sum_{j=MES,MAC} \xi^{Z_j} \sum_k g_{F_k}^{Z_j} * Z_j * F_k \frac{Fe_{F_k}}{F_k}}_{unassimilated\ food} \\
&+ \underbrace{\phi_{agg}^{POC \to GOC} \frac{SFE}{POC}}_{Fe\ aggregation} - \underbrace{\lambda_{GOC}^* Fe}_{remineralisation} - \underbrace{V_{sink} \frac{\partial BFE}{\partial z}}_{sinking\ of\ BFE}
\end{aligned} \tag{40}$$

$$\begin{aligned}
\frac{\partial SFE}{\partial t} &= \underbrace{Fe_{scave} * (POC + GOC + DSI + CAL) * POC}_{scavenging} \\
&- \underbrace{\sum_j g_{POC}^{Z_j} * Z_j * POC \frac{SFE}{POC}}_{grazing\ loss} + \underbrace{\xi^{MIC} \sum_k g_{F_k}^{MIC} * MIC * F_k \frac{Fe_{F_k}}{F_k}}_{unassimilated\ food} \\
&- \underbrace{\phi_{agg}^{POC \to GOC} \frac{SFE}{POC}}_{Fe\ aggregation} - \underbrace{\lambda_{SFe}^* BAC}_{remineralisation} - \underbrace{S_{POC} \frac{\partial SFE}{\partial z}}_{sinking\ of\ SFE} + \underbrace{\left(\frac{Fe}{C}\right)_Z POC_{riv}}_{river\ input}
\end{aligned} \tag{41}$$

The remineralisation λ_{SFe}^* is given by equation 23. Fe_{scav} is described below.

6.1.3 Dissolved Fe - FER

The temporal evolution of dissolved iron, FER, is calculated as follows:

$$\begin{aligned}
\frac{\partial FER}{\partial t} &= \underbrace{-\mu_{opt}^{P_i}(1 + \delta^{P_i}) f(T) L_{Q_{Fe}}^{P_i} L_{nutFe}^{P_i} P_i}_{production} + \underbrace{\mu_{opt}^{P_i} \delta_{P_i} f(T) L_{Q_{Fe}}^{P_i} L_{nutFe}^{P_i} P_i}_{loss} \\
&+ \underbrace{\sum_j \left(\sum_k g_{f_k}^{z_j} * Z_j * F_k \frac{Fe_{F_k}}{F_k} (1 - \xi^{Z_j}) - \left(\frac{Fe}{C}\right)_Z \sum_k g_{F_k}^{Z_j} * Z_j * F_k * MGE^{Z_j} \right)}_{grazing} \\
&+ \underbrace{FER_{remin_BFE_SFE}}_{mineralisation} - \underbrace{FER_{BAC}}_{bacterial\ uptake} - \underbrace{Fe_{scav}}_{scavenging} + \underbrace{Fe_{dep}}_{dust\ deposition} + \underbrace{Fe_{riv}}_{river\ input}
\end{aligned} \tag{42}$$

Iron is input from rivers, see Section 8.6, and the dissolution of dust from the atmosphere, see Section 8.5. Iron is taken up by phytoplankton during primary production (see above). When iron concentration is above 0.6 nM, it is scavenged by POM: the evolution of scavenged iron, Fe_{scav} is calculated as:

$$\begin{aligned} Fe_{scav} &= k_{scm} + k_{sc} * (POC + GOC + CAL + DSI) * 1e6 \\ &* \frac{-(1 + l_{Fe}k_{eq} - FERk_{eq}) + ((1 + l_{Fe}k_{eq} - FERk_{eq})^2 + 4FERk_{eq})^{0.5}}{2k_{eq}} \end{aligned} \tag{43}$$

where k_{scm} and k_{sc} are scavenging parameters and k_{eq} is given by:

$$k_{eq} = 10^{17.27 - \frac{1565.7}{T-19}}. \tag{44}$$

The iron ligand, l_{Fe} is set to a value of $.6 * 10^{-}9$ at latitudes North of 30S and below 200m depth, $.3 * 10^{-}9$ South of 40S and below 200 m, 0 above 100m depth, and linearly interpolated in between. Part of the scavenged iron is added to POM, and part is removed from the model.

Bacterial iron demand is

$$BAC\_Fe\_demand = BGE \left(\frac{Fe}{C}\right)_H * (\lambda^*_{DOC} + \lambda^*_{POC} + \lambda^*_{GOC}) * BAC \tag{45}$$

Bacterial iron supply is

$$BAC\_Fe\_supply = (\lambda^*_{SFe} + \lambda^*_{BFe}) * BAC \tag{46}$$

If supply exceeds demand, the rest contributes to FER:

$$FER_{remin\_BFE\_SFE} = MAX(BAC\_Fe\_supply - BAC\_Fe\_demand, 0.) \tag{47}$$

If demand exceeds supply, it draws on dissolved iron (FER):

$$FER_{BAC} = MAX((BAC\_Fe\_demand - BAC\_Fe\_supply) \frac{FER}{K^{BAC}_{FER} + FER}, 0.) \tag{48}$$

If there is not enough FER to meet this demand, BGE is decreased (Eq. 25).

6.2 The Silicate cycle

Silica is input from rivers and the dissolution of dust from the atmosphere. Growth of diatoms consumes dissolved silica (SIL) from the water to produce hydrated silica (biogenic silica BSI). Loss processes of diatoms produce sinking particulate silica (DSI).

Table 12: List of parameters and variables used to calculate the evolution of iron

Term	Variable	Description	Defined in
$FER_{remin\_BFE\_SFE}$	rbafer	Release of dissolved Fe by bacteria	bgcsnk.F90
Fe_{scav}	xscave	Iron scavenged by particulate organic matter	bgcsnk.F90
Fe_{riv}	depfer	River deposition	trcini
Fe_{dep}	irondep	Dust deposition	bgcbio.F90
k_{sco}	rn_scofer	Scavenging rate for iron by particles	namelist.trc.sms
k_{scm}	rn_scmfer	Minimum scavenging rate for iron	namelist.trc.sms
k_{eq}	xkeq	Scavenging rate parameter	bgcsnk.F90
l_{Fe}	ligfer	iron ligand concentration	bgcsnk.F90

6.2.1 Dissolved SiO_3 - SIL

The temporal evolution of dissolved silica is calculated as:

$$\begin{aligned}\frac{\partial SIL}{\partial t} &= \underbrace{\left(\frac{Si}{C}\right)_{DIA} \mu^{DIA} DIA}_{production} + \underbrace{\beta_{Si} DSI}_{dissolution} \\ &+ \underbrace{SIL_{riv}}_{river\ input} + \underbrace{SIL_{dep}}_{dustdeposition}\end{aligned} \tag{49}$$

where $\mu^{DIA} DIA$ is the primary production, in terms of carbon, of diatoms, β_{Si} is the remineralisation rate of silica which is dependent on temperature, T and oxygen OXY (equation 24):

$$\beta_{Si} = \min\left(rem_{DSI} e^{\frac{ret_{DSI}}{(273.15+T)}}, rem_{max,DSI}\right) \eta_O. \tag{50}$$

$\left(\frac{Si}{C}\right)_{DIA}$ increases with iron stress and silicate availability:

$$\left(\frac{Si}{C}\right)_{DIA} = max(\left(\frac{Si}{C}\right)_{FER}, \left(\frac{Si}{C}\right)_{SIL}) \tag{51}$$

$$\left(\frac{Si}{C}\right)_{FER} = 1. + \left(\frac{BSi}{DIA}\right)_{FER} * min\left(\frac{SIL}{K_{SIL}^{DIA}}, 1\right) * (1 - min\left(\frac{FER}{K_{FER}^{DIA}}, 1\right)). \tag{52}$$

where K_{SIL}^{DIA} and K_{FER}^{DIA} are the half saturation constant for SiO_3 and Fe in diatoms. Observations in the Southern Ocean show a high $\left(\frac{Si}{C}\right)_{DIA}$ ratio in areas with very high Si concentration so $\left(\frac{Si}{C}\right)_{DIA}$ is arbitrarily increased

throughout the ocean to reflect this:

$$\left(\frac{Si}{C}\right)_{SIL} = \left(\frac{BSi}{DIA}\right)_{SIL} * \frac{SIL}{SIL + K_{BSI}}. \tag{53}$$

$\left(\frac{Si}{C}\right)_{DIA}$ is set to the higher of these two ratios. SIL_{dep} is described in 8.5 and SIL_{riv} in 8.6.

Equation (53) is inherited from PISCES [Aumont, 2005] and derived from Equation (8) of Jeandel et al. [1998].

Table 13: List of parameters and variables used to calculate the evolution of silica

Term	**Variable**	**Description**	**Defined in**
β_{Si}	siremin	remineraliation rate of silica (d^{-1})	bgcsnk.F90
$(\frac{BSi}{DIA})_{FER}$	rn_ferbsi	$(\frac{Si}{C})_{DIA}$ increase under Fe limitation	namelist.trc.sms
$(\frac{BSi}{DIA})_{SIL}$	rn_silbsi	$(\frac{Si}{C})_{DIA}$ increase under SiO3 limitation	namelist.trc.sms
$\mu^{DIA}DIA$	prophy	primary production of diatoms (mol (L timestep)$^{-1}$)	bgcpro.F90,bgcnul.F90
$(\frac{Si}{C})_{DIA}$	silfac	Si/C ratio of diatoms	bgcpro.F90
K_{FER}^{DIA}	rn_kmfphy	half saturation constant of Fe	namelist.trc.sms
K_{SIL}^{DIA}	rn_sildia	half saturation constant of SiO3	namelist.trc.sms
K_{BSI}	rn_kmsbsi	half saturation constant for $\left(\frac{Si}{C}\right)$	namelist.trc.sms
rem_{DSI}	rn_remdsi	remineralisation of DSI	namelist.trc.sms
ret_{DSI}	rn_retdsi	temperature depend. remineral. of DSI	namelist.trc.sms
$rem_{max,DSI}$	rn_readsi	max. remineralisation of DSI	namelist.trc.sms
$(\frac{Si}{C})_{min}$	rn_bsidia	minimum $(\frac{Si}{C})_{DIA}$	namelist.trc.sms
SIL_{riv}	depsil	river input of SiO_3	trcini
SIL_{dep}	sidep	input of atmospheric silica to the water column	bgcbio.F90

6.2.2 Biogenic particulate silica - BSI

The temporal evolution of biogenic silica is calculated as:

$$\begin{aligned} \frac{\partial BSI}{\partial t} &= \underbrace{\left(\frac{Si}{C}\right)_{min}\left(\frac{Si}{C}\right)_{DIA}\mu^{DIA}DIA}_{production} \\ &- \underbrace{\sum_j g_{DIA}^{Z_j} * Z_j * DIA\frac{BSI}{DIA}}_{grazing} - \underbrace{\delta_{DIA}\mu_0^{DIA}b^T\frac{BSI}{DIA}}_{loss} \end{aligned} \tag{54}$$

where δ^{DIA} is the fraction of diatom production that is respired/lost, and $\left(\frac{Si}{C}\right)_{DIA}$ is described above.

6.2.3 Sinking particulate silica - DSI

The temporal evolution of sinking particulate silica is calculated as:

$$\begin{aligned}\frac{\partial DSI}{\partial t} &= \underbrace{\delta_{DIA}\mu_0^{DIA}b^T\frac{BSI}{DIA}}_{loss} - \underbrace{\beta_{Si}DSI}_{dissolution} \\ &+ \underbrace{\sum_j g_{DIA}^{Z_j} * Z_j * DIA\frac{BSI}{DIA}}_{grazing} + \underbrace{V_{sink}\frac{\partial DSI}{\partial z}}_{sinking\ DSI}\end{aligned} \tag{55}$$

6.3 Phosphorus and Nitrogen - PO4, NH4 and NO3

Phosphate is input to the ocean by river deposition; it is consumed during phytoplankton growth and produced during respiration.

$$\frac{\partial PO4}{\partial t} = \underbrace{\sum -\mu^{P_i}P_i\left(1+\nu_{P_i}^{tot}\right)\frac{P}{C}}_{production} + \underbrace{consum\frac{P}{C}}_{remineralisation} + \underbrace{PO4_{riv}}_{river\ input} \tag{56}$$

$consum$ is defined in equation 37.

Dissolved ammonium evolves as:

$$\begin{aligned}\frac{\partial NH4}{\partial t} &= \underbrace{\sum -\mu^{P_i}P_i(1+\nu_{p_i}^{tot})\frac{N}{C}DIN_{NH4}}_{production} + \underbrace{consum\frac{N}{C}}_{remineralisation} \\ &- nitrification + \underbrace{NHy_{riv}\frac{N}{C}}_{river\ input} + \underbrace{NHy_{atm}}_{atmosphere\ deposition}\end{aligned} \tag{57}$$

For phytoplankton other than nitrogen fixers:

$$DIN_{NH4} = \frac{NH_4}{(NH_4 + K_{NH4}^{P_i})dinlim} \tag{58}$$

and for nitrogen fixers:

$$DIN_{NH4} = \frac{NH_4}{(NH_4 + K_{NH4}^{P_i})(dinlim + R_{fix}(1-dinlim))} \tag{59}$$

dinlim is defined in Eq. 10.

$$\begin{aligned}nitrification &= r_{nitrif} * max((1 - log(OXY * 1e6) * 0.159)(1 - resp_{BAC}^{NO_3}), 0) \\ &* \frac{NH4}{NH4 + K_{nitrif}} * d_{BAC}^T * NH4\end{aligned} \tag{60}$$

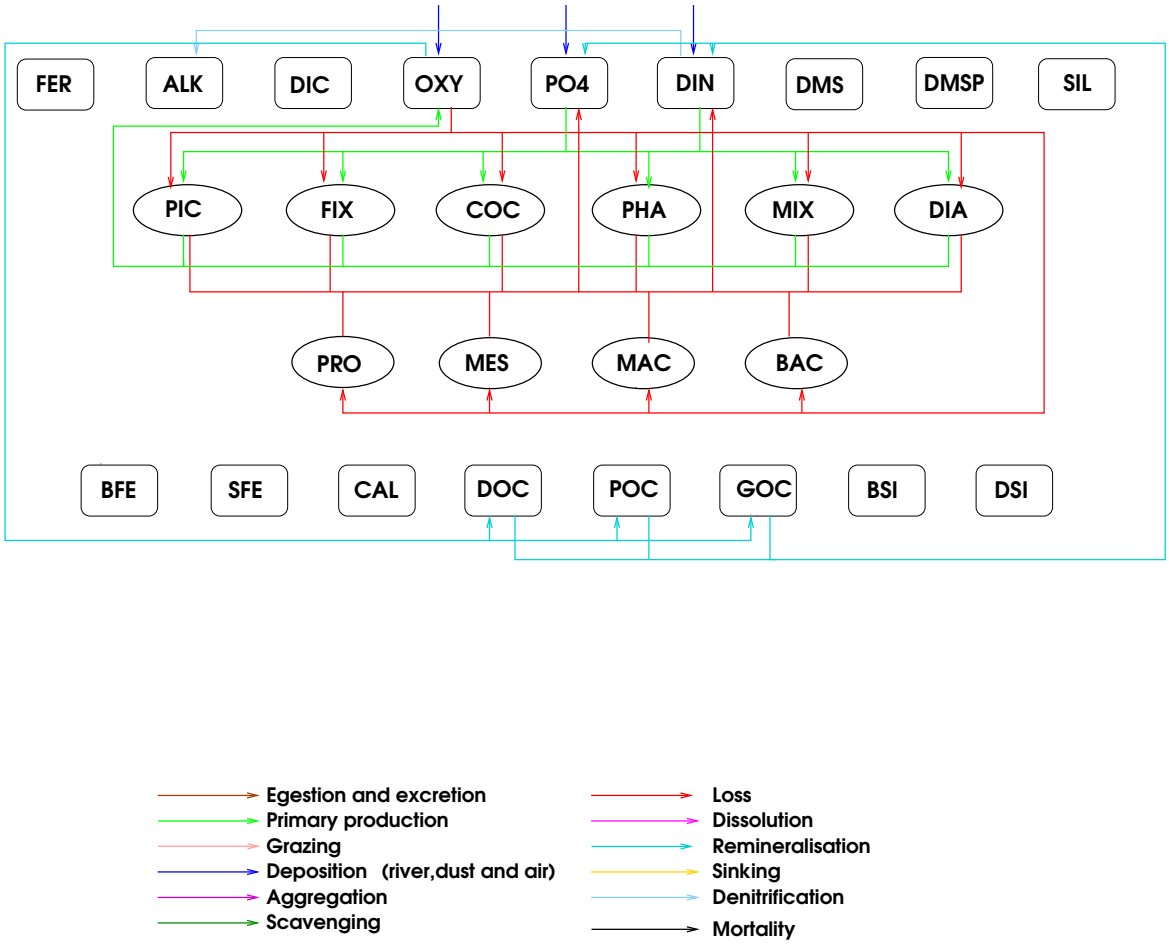

Figure 7: The sources and sinks for phophate (PO4), nitrogen (DIN=NH4+NO3), oxygen (OXY)).

Dissolved nitrate evolves as:

$$\frac{\partial NO3}{\partial t} = \underbrace{\sum -\mu^{P_i} P_i (1+\nu_{p_i}^{tot}) \frac{N}{C} DIN_{NO3}}_{production} - \underbrace{N_{denit}}_{denitrification} + \text{nitrification} + \underbrace{NOx_{riv}\frac{N}{C}}_{river\ input} + \underbrace{NOx_{atm}}_{atmosphere\ deposition} \tag{61}$$

where

$$N_{denit} = 0.8\left(\frac{O}{C} * consum * resp_{BAC}^{NO_3}\right). \tag{62}$$

$\frac{O}{C} = \frac{172}{122}$ and $resp_{BAC}^{NO_3}$ is the fraction of bacterial respiration that uses NO_3 rather than O_2 and is described in Section 6.4. For phytoplankton other than nitrogen fixers:

$$DIN_{NO3} = \frac{NO_3(1-\frac{NH_4}{NH_4+K_{NH4}^{P_i}})}{(NO_3+K_{NO3}^{P_i})dinlim} \tag{63}$$

and for nitrogen fixers:

$$DIN_{NO3} = \frac{NO_3(1-\frac{NH_4}{NH_4+K_{NH4}^{P_i}})}{(NO_3+K_{NO3}^{P_i})(dinlim+R_{fix}(1-dinlim))} \tag{64}$$

6.4 Oxygen - OXY

Oxygen is produced during the growth of phytoplankton. It is consumed during the growth of N_2 fixers on N_2 and during the remineralisation described by the term $consum$ in Section 5.2. There is also an exchange of oxygen with the atmosphere.

$$\frac{\partial OXY}{\partial t} = \underbrace{\frac{O}{C}\sum \mu^{P_i} P_i \left(1+\nu_{P_i}^{tot}\right)}_{phytoplankton\ growth} - \underbrace{\frac{N}{C}\mu^{P_{fix}} P_{fix}\left(1+\nu_{FIX}^{tot}\right)1.25(1-DIN_{nit})}_{growth\ of\ N_2\ fixers\ on N_2} - \underbrace{\frac{O}{C} consum(1-resp_{BAC}^{NO_3})}_{remineralisation} + \underbrace{F_{air-sea}^{O_2}}_{O_2\ flux\ from\ air\ to\ sea} \tag{65}$$

The fraction of bacterial respiration that uses NO_3 rather than O_2, $resp_{BAC}^{NO_3}$ is given by:

$$resp_{BAC}^{NO_3} = \frac{\sin\left(\max\left(-.5, \frac{8.5E-6-OXY}{17E-6+OXY}\right) * \pi\right)+1}{2} \tag{66}$$

Table 14: List of Parameters used in the evolution of phosphate and nitrogen

Term	Variable	Description	Defined in
DIN_{NH4}	1-dinpft	fraction of phyto growth that is supported by NH4	bgcpro.F90
DIN_{NO3}	dinpft	fraction of phyto growth that is supported by NO3	bgcpro.F90
$K^{P_i}_{NH4}$	rn_kmhphy	NH_4 half saturation constants for phytoplankton	namelist.trc.sms
K_{nitrif}	rn_kmhnit	NH_4 half saturation constant nitrification	namelist.trc.sms
$K^{P_i}_{NO3}$	rn_kmnphy	NO_3 half saturation constants for phytoplankton	namelist.trc.sms
$\frac{N}{C}$	ratn2c	N:C ratio organic matter = 16:122	trcini
N_{denit}	denitr	denitrification	bgcbio.F90
NHy_{atm}	atmamm	Atmosphere input of NH_y	trcini
NHy_{riv}	depamm	River input of NH_y	trcini
NOx_{atm}	atmnit	Atmosphere input of NO_x	trcini
NOx_{riv}	depnit	River input of NO_x	trcini
$PO4_{riv}$	deppo4	River input of phosphate	trcini
R_{FIX}	rn_munfix	Fraction of growth rate during N_2 fixation relative to growth on fixed N	namelist.trc.sms
r_{nitrif}	rn_nitnh4	NH4 saturated nitrification rate at 0 C	namelist.trc.sms
$resp^{NO_3}_{BAC}$	nitrfac	fraction of bacterial respiration using NO_3 rather than O_2	bgcnul.F90

The air-sea exchange of oxygen, $F^{O_2}_{air-sea}$, is given by

$$F^{O_2}_{air-sea} = \left(\frac{O}{N}_{pi} sol_{O_2} \left(1. - e^{20.1050 - 0.0097982 * sstk - 6163.10/sstk} \right) - OXY \right) 0.27 v^2 (1 - \gamma) \quad (67)$$

The terms are described described in Section 7. It is calculated in bgcflx.F90.

6.5 Diagnostic nitrous oxide - N2S

The diagnostic formulation of nitrous oxide production is a function of O_2 consumption, with a yield that depends on the oxygen concentration. Under oxic conditions, there is a constant yield, while under suboxic conditions the yield increases as oxygen decreases :

$$\frac{\partial N2S}{\partial t} = (\alpha_{N_2O} + \beta_{N_2O} * exp(-0.1 * \frac{OXY - 1e-6}{1e-6})) * \frac{O}{C} consum(1 - resp^{NO_3}_{BAC}) \quad (68)$$

6.6 Prognostic nitrous oxide - N2O

The prognostic formulation of nitrous oxide production is a function of redox reactions in the nitrogen cycle.

$$\frac{\partial N2O}{\partial t} = (y_{nitrif} * nitrification + y_{denitr} * N_{denit} - y_{N2Ocons} * N_{N2Ocons} \quad (69)$$

$$N_{N2Ocons} = 0.8 \left(\frac{O}{C} * consum * \frac{\sin\left(\max\left(-.5, \frac{7E-6-OXY}{14E-6+OXY}\right) * \pi\right) + 1}{2} \right) \quad (70)$$

Table 15: List of Parameters used in the evolution of N2S and N2O

Term	Variable	Description	Defined in
α_{N_2O}	rn_aoun2s	yield of oxic N2O production	namelist.trc.sms
β_{N_2O}	rn_betn2s	yield of suboxic N2O production	namelist.trc.sms
$consum$	consum	remineralisation rate	Eq. 37 , bgcnul.F90
N_{denit}	denitr	denitrification	Eq. 62 , bgcbio.F90
$N_{N2Ocons}$	degn2o	N2O consumption rate/$y_{N2Ocons}$	Eq. 70 , bgcbio.F90
$nitrification$	nitrif	nitrification rate	Eq. 60 , bgcbio.F90
$\frac{O}{C}$	rato2c	-O2:C ratio = 172:122	trcini
$resp_{BAC}^{NO_3}$	nitrfac	fraction of bacterial respiration using NO_3 rather than O_2	Eq. 66 , bgcnul.F90
$y_{N2Ocons}$	rn_degn2o	yield of N2O consumption	namelist.trc.sms
y_{denitr}	rn_denn2o	N2O yield of denitrification	namelist.trc.sms
y_{nitrif}	rn_aoun2o	N2O yield of nitrification	namelist.trc.sms

6.7 Methane - CH4

Several formulations of methane cycling were tested: Formulation (1), (4) and (7): production is proportional to metazoan zooplankton fecal pellet production:

$$\frac{\partial CH4}{\partial t} = y_{fecpel} * \underbrace{\sum_j \xi^{Z_j} \sum_k g_{F_k}^{Z_j} * Z_j * F_k}_{zooplankton\ unassimilated\ food} \quad (71)$$

Formulations (1) has a globally invariant y_{fecpel}, in formulation (4) y_{fecpel} = 0 below 2000m, and formulation (7) has a different y_{fecpel} in the open ocean above 2000m and in the coastal ocean.

Formulation (2): production is proportional to O_2 consumption:

$$\frac{\partial CH4}{\partial t} = y_{respir} * \underbrace{\frac{O}{C} consum(1 - resp_{BAC}^{NO_3})}_{remineralisation} \quad (72)$$

Formulation (3):

$$\frac{\partial CH4}{\partial t} = y_{fecpel} * \sum_j \xi^{Z_j} \sum_k g_{F_k}^{Z_j} * Z_j * F_k - y_{respir} * \frac{O}{C} consum(1 - resp_{BAC}^{NO_3}) \quad (73)$$

Formulation (5):

$$\frac{\partial CH4}{\partial t} = y_{fecpel} * \sum_j \xi^{Z_j} \sum_k g_{F_k}^{Z_j} * Z_j * F_k + y_{respir} * \frac{O}{C} consum(1 - resp_{BAC}^{NO_3}) \quad (74)$$

with y_{fecpel} = 0 below 2000m, and y_{respir} = 0 everywhere except the bottom water layer.

Formulation (6):

$$\frac{\partial CH4}{\partial t} = y_{fecpel} * \sum_j \xi^{Z_j} \sum_k g_{F_k}^{Z_j} * Z_j * F_k + y_{hypoxic} * exp(-0.1 * \frac{OXY - 1e-6}{1e-6})) * \frac{O}{C} consum(1 - resp_{BAC}^{NO_3}) \quad (75)$$

7 Air-sea exchange of gases

The air-sea flux of gases (CO_2, O_2, and optionally DMS, N_2O and/or CH_4) is given by the product of gas exchange coefficient and the difference in concentration of the gas across the sea-air interface:

$$F_{air-sea} = k_w * (1 - \gamma) * (pC_{gas}^{air} - pC_{gas}^{sea}) \quad (76)$$

where k_w is the gas exchange coefficient, γ is the fraction of the ocean covered by ice, pC_{gas}^{air} is the concentration of the gas in the air directly above the water, and pC_{gas}^{sea} is the sea surface concentration of the gas.

The gas exchange coefficient is calculated according to Wanninkhof [1992] (eq. 3):

$$k_w = 0.27 * v^2 * \sqrt{660./Schmidt_{gas}} \quad (77)$$

where v is the amplitude of the winds (m/s), sst is the sea surface temperature, and Schmidt$_{gas}$ is the Schmidt number for each gas Wanninkhof [1992].

7.1 CO_2

For the gas exchange coefficient CO_2 Wanninkhof [1992] include a chemical enhancement term:

$$k_w^{CO_2} = 0.27 * v^2 + 2.5 * (0.5246 + 0.016256 * sst + 0.00049946 * sst^2) \quad (78)$$

For CO_2, $pC_{CO_2}^{air}$ is calculated from the measured mixing ratio of CO_2 in the atmosphere ($C_{CO_2}^{air}$, in ppm) times the solubility of CO_2 in sea water and corrected for 100% water vapor Sarmiento et al. [1992]:

$$pC_{CO_2}^{air} = C_{CO_2}^{air} * sol_{CO_2} * (1. - e^{20.1050 - 0.0097982 * sstk - 6163.10/sstk}) \quad (79)$$

where sstk is sea surface temperature in degree Kelvin. The solubility of CO_2 is given by:

$$sol_{CO_2} = e^{c00 + c01/(sstk*.01) + c02*\ln(sstk*.01) + sal*(c03 + c04*qtt + c05*(sstk*.01)^2)} * smicr \quad (80)$$

where sal is the salinity and the coefficents $c00$, $c01$, $c02$, $c03$, $c04$, $c05$ and $smicr$ are given by Wanninkhof [1992]. The Schmidt number for CO_2 is given by:

$$Schmidt_{CO_2} = 2073.1 - 125.62 * sst + 3.6276 * sst^2 - 0.043126 * sst^3 \tag{81}$$

$C^{sea}_{CO_2}$ is the concentration of CO_2 in the model, calculated based on the state variables DIC and TALK.

7.2 O_2

For O_2, $pC^{air}_{O_2}$ is calculated from the measured mixing ratio of O_2 in the atmosphere ($C^{air}_{O_2}$, times the solubility of O_2 in seawater, also corrected for 100% water vapor as for CO_2 Sarmiento et al. [1992]:

$$pC^{air}_{O_2} = C^{air}_{O_2} * sol_{O_2} * (1. - e^{20.1050 - 0.0097982 * sstk - 6163.10/sstk}) \tag{82}$$

The solubility of O_2 is calculated as follows:

$$\begin{aligned} sol_{O_2} &= e^{ox0 + ox1/(sstk*.01) + ox2*\ln(sstk*.01) + sal*(ox3 + ox4*(sstk*.01) + ox5*(sstk*.01)^2)} \\ &* \quad oxyco \end{aligned} \tag{83}$$

The Schmidt number for O_2 is given by:

$$Schmidt_{O_2} = 1953.4 - 128.0 * sst + 3.9918 * sst^2 - 0.050091 * sst^3 \tag{84}$$

where sal is the salinity and the coefficents $ox0$, $ox1$, $ox2$, $ox3$, $ox4$, $ox5$, and $oxyco$ are given by Wanninkhof [1992].

7.3 N_2O

pN_2O uses the same water vapor correction as CO_2.

The solubility of N_2O is calculated as follows (Weiss and Price 1980):

$$\begin{aligned} sol_{N_2O} = e^{(&-62.7062 + 97.3066/(sstk*.01) + 24.1406*\ln(sstk*.01) \\ &+ sal*(-0.058420 + 0.0331983*(sstk*.01) - 0.0051313*(sstk*.01)^2)) \end{aligned} \tag{85}$$

The Schmidt number for N_2O is given by Wanninkhof [1992]:

$$Schmidt_{N_2O} = 2301.1 - 151.1 * sst + 4.7364 * sst^2 - 0.059431 * sst^3 \tag{86}$$

7.4 CH_4

pCH_4 uses the same water vapor correction as CO_2.

The solubility of CH_4 is calculated as follows (Wiesenburg and Guinasso 1979):

$$sol_{CH_4} = e^{(-415.2807+596.8104/(sstk*.01)+379.2599*\ln(sstk*.01)-62.0757*(sstk*.01) \\ +sal*(-0.059160+0.032174*(sstk*.01)-0.0048198*(sstk*.01)^2))} \quad (87)$$

The Schmidt number for CH_4 is given by Wanninkhof [1992]:

$$Schmidt_{CH_4} = 2039.2 - 120.31 * sst + 3.4209 * sst^2 - 0.040437 * sst^3 \quad (88)$$

Table 16: List of parameters and variables used to calculate the evolution of air-sea fluxes

Term	Variable	Description	Defined in
v	wndm	wind speed	
sal	sn(1)	salinity of sea surface layer	
sst	tn(1)	temperature of sea surface (°C)	
$c00$	c00	coefficient in the solubility of CO2	trcini
$Schmidt_{CO_2}$	schmico2	Schmidt number for CO_2	bgcflx.F90
$Schmidt_{O_2}$	schmio2	Schmidt number for O_2	bgcflx.F90
γ	freeze	fraction of ocean covered by ice	ice model Section 8.2
$\frac{O}{N}^{pi}$	atcox	pre-industrial ratio of oxygen to nitrogen	trcini
$F^{O_2}_{air-sea}$	flu16	air-sea oxygen flux	bgcflx.F90

8 Model Setup

8.1 Ocean General Circulation Model

The physical model NEMO v3.1 (Madec [2008],
http://www.nemo-ocean.eu/About-NEMO/Reference-manuals) was developed by the Laboratoire d' Océanographie Dynamique et de Climatologie (LODYC) to study large scale ocean circulation and its interaction with atmosphere and sea-ice. NEMO is based on the Navier-Stokes equations describing the motions of the fluid and on a non-linear equation of state, which couples the two tracers salinity and temperature to the fluid velocity.

8.2 Sea-Ice Model

NEMO is coupled to the Louvain-La-Neuve Sea-Ice Model (LIM, Timmermann et al., 2005), developed by Fichefet and Morales-Maqueda [1999]. LIM has been thoroughly validated for both Arctic and Antarctic conditions, and has been used in a wide range of process studies. Due to the use of an elaborate technique for solving the continuity

equations [Prather, 1986], LIM is particularly suited to describing the ice-edge in coarse grid resolutions, which are typically used for climate modelling studies. The physical fields that are advected in LIM are the ice concentration, the snow volume per unit area, the ice volume per unit area, the snow enthalpy per unit area, the ice enthalpy per unit area, and the brine reservoir per unit area. A full model description and details of the coupling to OPA-ORCA can be found in Timmermann et al. [2005].

8.3 Forcing

8.3.1 Physical Forcing

The model is forced by daily wind stress, cloud cover and precipitation from the NCEP/ NCAR reanalysed fields [Kalnay et al., 1996]. Sensible and latent heat fluxes are calculated with bulk formulae using the differences between the surface temperature calculated by OPA and the observed air temperature, taking into account local humidity. At the end of each year a water balance is calculated and a uniform water flux correction is applied during the following year to conserve the water mass.

8.4 Initialisation

All model simulations are initialized with observations from the World Ocean Atlas 2009 for temperature [Locarnini et al., 2010], salinity [Antonov et al., 2010] PO_4^{3-},NO_3^-, SiO_3^-, [Garcia et al., 2010b] and O_2 [Garcia et al., 2010a]. DIC, alkalinity (GLODAP) observations were from Key et al. [2004]. The biological state variables are initialised with the output from previous model runs.

8.5 Dust input

The model is forced with Fe and Si input from monthly dust fluxes taken from Jickells et al. [2005] and interpolated to daily values in bgcint.F90. The input is total dust rather than in units of Fe. We assume 0.035g Fe per g of dust and either 8.8g Si per g Fe or, the equivalent, 0.308 g Si per g dust. The solubility of Fe in dust is generally taken to be 2 % and may be set in rn_fersol. The solubility of Si in dust is 7.5 %. Using these values the dust is converted to equivalent Fe, Fe_{dep} and Si, Si_{dep} in units of mol/L/timestep in bgcbio.F90.

8.6 River input

Annual fluxes of riverine carbon and nutrient (N, Si, Fe) to the ocean were computed following a global river drainage direction map (DDM30), considering population and basin area [Döll and Lehner, 2002], and river runoff [Kourzoun, 1977, Ludwig and Probst, 1998] at 0.5° increments of latitude and longitude as in da Cunha et al. [2007]. This map represents the drainage directions of surface water on all continents, except Antarctica. Cells of the map are connected by their drainage directions and are thus organized into drainage basins. We use the cells corresponding to basin outlets to the ocean as input data for PlankTOM.

Values for DIC_{riv}, DOC_{riv}, POC_{riv}, NHy_{riv}, NOx_{riv}, $PO4_{riv}$, SIL_{riv} and Fe_{riv} as used in the preceding Sections are obtained by multiplying the input by the relevant parameter in Table 17. Thus all riverine inputs may be switched off by setting their parameter to zero.

In order to close the N, Si, and alkalinity cycles of the ocean, as much POM, DOM, SiO2 and CaCO3 is removed from the bottom water layer as is added by rivers and Si in dust.

8.6.1 Dissolved Inorganic Nitrogen (DIN)

To calculate riverine DIN inputs we used a regression model originally developed by Smith et al. [2003]:

$$\log DIN = 3.99 + 0.35 \log POP + 0.75 \log R \tag{89}$$

where (DIN) is in mol N km^{-2} y^{-1}, (POP) is population density in people km^{-2}, and (R) is runoff in m y^{-1}. The model describes DIN export by the analysis of 165 systems for which DIN flux data is available [Meybeck and A., 1997], S. Smith and F. Wulff (Eds.), LOICZ-Biogeochemical modelling node, 2000, available at http://data.ecology.su.se/MNODE/]. In this model, riverine DIN export to the coastal zone is a function of basin population density and runoff: On the basis of basin area, basin population (for the year 1990) and runoff provided by the DDM30 map, 16.3 Tg DIN y^{-1} (1.16 Tmol N y^{-1}) are transported to the coastal zone by rivers. In the Smith et al. 2003 model, the average N:P ratio of riverine export is 18:1, which is close to the PISCES-T N:P ratio of 16:1. Nitrogen retention in estuarine areas was not included owing to lack of global data.

8.6.2 Dissolved Silica (Si)

Rivers are responsible for 80% of the inputs of Si to the ocean [Treguer et al., 1995]. For an estimate of riverine input of dissolved Si we used the runoff data from the DDM30 map, and applied an average concentration of Si in river waters of 4.2 mg Si/L [Treguer et al., 1995]. Si concentration in river water is variable according to basin geology but regional data is not available. Our estimate leads to a dissolved Si river input of 187 Tg Si y^{-1} to the ocean. This value is comparable to the range of 140 $\pm$ 30 Tg Si y^{-1} for a net riverine dissolved Si input to the ocean proposed by Treguer et al. [1995], considering estuarine retention of Si.

8.6.3 Dissolved Iron (Fe)

Rivers and continental shelf sediments supply Fe to surface waters. Because it is extensively removed from the dissolved phase in estuaries, rivers are thought to be a minor source for the open ocean, but not for coastal zones. We used the runoff data from the DDM30 map and applied an average concentration of dissolved Fe in river waters of 40 mg L^{-1} [Martin and Meybeck, 1979, Martin and Whitfield, 1983]. As for Si, river basin geology influences Fe concentration in river water, but there is no available global database on riverine Fe. Our estimate leads to a gross dissolved Fe input of 1.75 Tg Fe y^{-1}, comparable to the estimate of 1.45 Tg Fe $^{-1}$ by Chester [1990].

During estuarine mixing, flocculation of colloidal Fe and organic matter forms particulate Fe because of the major change in ionic strength upon mixing of fresh water and seawater [de Baar and Jong, 2001]. This removal has been well documented in many estuaries. Literature values show that approximately 80 to 99% of the gross

dissolved Fe input is lost to the particulate phase in estuaries at low salinities [Boyle et al., 1977, Chester, 1990, Dai and Martin, 1995, Lohan and Bruland, 2006, Sholkovitz, 1978].

We apply a removal rate of 99% to our gross Fe flux, and obtained a net input of riverine dissolved Fe to the coastal ocean of 0.02 Tg Fe y^{-1}.

8.6.4 Particulate (POC) and Dissolved Organic (DOC) and Inorganic (DIC) Carbon

The predicted river carbon fluxes are based on models relating river carbon fluxes to their major controlling factors [Ludwig and Probst, 1998, Ludwig et al., 1996b]. For POC, sediment flux is the dominant controlling parameter. For DOC, runoff intensity, basin slope, and the amount of soil OC in the basin are the controlling parameters [Ludwig et al., 1996b]. We applied this model to the DDM30 data set, and we estimate a gross discharge of 148 Tg C y^{-1} and 189 Tg C y^{-1} for POC and DOC, respectively. We assume that DOC has a conservative behavior in estuaries. These values are in agreement with recent modeled values of 170 Tg C y^{-1} as DOC [Harrison et al., 2005], and 197 Tg C y^{-1} as POC [Beusen et al., 2005, Seitzinger et al., 2005]. We used a C:N:P:Fe ratio of 122:16:1:2.44 10^{-4}, thus riverine DOC and POC, when they are remineralized, are also N, P and Fe sources to the ocean. Inorganic carbon is mainly transported by rivers in the dissolved form. For DIC inputs, drainage intensity and river basin lithology are the controlling parameters [Ludwig et al., 1996a]. We applied this model to the DDM30 data set, and we estimate a DIC and alkalinity discharge of 385 Tg C y^{-1} (32.12 Tmol C y^{-1}).

Table 17: List of Parameters used in river input

Variable	Description	Defined in
rn_rivdic	river input of DIC	namelist.trc.sms
rn_rivdoc	river input of DOC	namelist.trc.sms
rn_rivfer	river input of Fe	namelist.trc.sms
rn_rivpoc	river input of POC	namelist.trc.sms
rn_rivnit	river input of nitrate	namelist.trc.sms
rn_rivpo4	river input of phosphate	namelist.trc.sms
rn_rivsil	river input of silica	namelist.trc.sms
rn_sedfer	coastal release of Fe	namelist.trc.sms

8.7 The namelist.trc.sms file

Values used for the parameters defined in namelist.trc.sms are given in the following tables.

Table 18: List of Parameters defined in namelist.trc.sms

Parameter	(optimised) value (and range)	Units	Description
rn_ag1poc	1.2e4	L s (mol d)$^{-1}$ m^{-2}	small POC (POC$_s$ aggregation
rn_ag2poc	1e4	L s (mol d)$^{-1}$ m^{-2}	POC$_s$ - large POC (POC$_l$) aggregation
rn_ag3poc	140	L (mol d)$^{-1}$	POC$_s$ - POC$_l$ aggregation
rn_ag4poc	150	L (mol d)$^{-1}$	POC$_s$ aggregation
rn_ag5doc	180	L s (mol d)$^{-1}$ m^{-2}	DOC - POC$_s$ aggregation
rn_ag6doc	3.9e3	L s (mol d)$^{-1}$ m^{-2}	DOC - POC$_l$ aggregation
rn_ag7doc	1e3	L s (mol d)$^{-1}$ m^{-2}	DOC - POC$_s$ aggregation
rn_alpphy	1.e-6	mol C m^2 (g Chl mol photons)$^{-1}$	initial slope of photsyntheses vs light intensity curve
rn_aoun2o	1.23e-4 (0.37e-4 - 2.53e-4)	mol N2O (mol NH4)$^{-1}$	N2O yield nitrification
rn_aoun2s	1.06e-5 (0.33e-5 - 2.26e-5)	mol N2O (mol O2)$^{-1}$	oxic N2S yield
rn_betn2s	1.7e-3 (1.7e-3 - 10.18e-3)	mol N2O (mol O2)$^{-1}$	suboxic N2S yield
rn_coccal	0.433	-	ratio of $CaCO_3$ to organic carbon
rn_degn2o	0 (0 - 9.65e-2)	mol N2O (mol NO3)$^{-1}$	yield N2O consumption
rn_denn2o	3.4e-3 (3.4e-3 - 80.8e-3)	mol N2O (mol NO3)$^{-1}$	N2O yield denitrification
rn_domphy	0.45	-	maximum DOC excretion ratio for all phyto
rn_discal	0.75	-	fraction of $CaCO_3$ dissolved during coccolithophore mortality
rn_docphy	0.05	-	excretion ratio for all phyto
rn_ekwgrn	0.0232	m^{-1}	green light absorption coefficient of H_2O
rn_ekwred	0.225	m^{-1}	red light absorption coefficient of H_2O
rn_etomax	80.	W m^{-2}	maximum surface insolation
rn_faco18	0.98	-	bacterial fractionation for O_{18}

Continued on next page

Table 18 – continued from previous page

Parameter	Value	Units	Description
rn_fersol	0.01	-	solubility of iron in dust
rn_gbadoc	0.088	-	relative preference of BAC grazing for DOC
rn_gbagoc	8.76	-	relative preference of BAC grazing for GOC
rn_gbagon	11.42	-	relative preference of BAC grazing for GON
rn_gbapoc	8.76	-	relative preference of BAC grazing for POC
rn_ggebac	0.21	-	growth efficiency BAC
rn_ggezoo	0.3	-	growth efficiency MAC
	0.25	-	growth efficiency MES
	0.29	-	growth efficiency PRO
rn_prfzoo	0.186	-	relative preference of MAC grazing for BAC
	0.186	-	relative preference of MAC grazing for GOC
	1.860	-	relative preference of MAC grazing for MES
	1.860	-	relative preference of MAC grazing for PRO
	1.860	-	relative preference of MAC for DIA
	1.860	-	relative preference of MAC for MIX
	1.860	-	relative preference of MAC for COC
	.930	-	relative preference of MAC for PIC
	1.860	-	relative preference of MAC for PHA
	.186	-	relative preference of MAC for FIX
	0.186	-	relative preference of MES grazing for POC
	.165	-	relative preference of MES grazing for BAC
	0.165	-	relative preference of MES grazing for GOC
	3.302	-	relative preference of MES grazing for PRO
	1.651	-	relative preference of MES for DIA
	1.238	-	relative preference of MES for MIX
	1.238	-	relative preference of MES for COC
	1.238	-	relative preference of MES for PIC
	1.238	-	relative preference of MES for PHA
	0.165	-	relative preference of MES for FIX
	0.165	-	relative preference of MES grazing for POC
	2.480	-	relative preference of PRO grazing for BAC
	0.062	-	relative preference of PRO grazing for GOC
	0.620	-	relative preference of MIC for DIA
	1.240	-	relative preference of MIC for MIX
	1.240	-	relative preference of MIC for COC
	1.240	-	relative preference of MIC for PIC
	1.240	-	relative preference of MIC for PHA
	1.240	-	relative preference of MIC for FIX

Continued on next page

Table 18 – continued from previous page

Parameter	Value	Units	Description
	0.062	-	relative preference of PRO grazing for POC
rn_grabac	3.15	d^{-1}	maximum BAC uptake rate
rn_grazoo	0.106	d^{-1}	maximum MAC grazing rate
	1.22	d^{-1}	maximum MES grazing rate
	1.59	d^{-1}	maximum PRO grazing rate
rn_grkzoo	9.e-6	mol L^{-1}	K_m for MAC grazing
	10.e-6	mol L^{-1}	K_m for MES grazing
	10.e-6	mol L^{-1}	K_m for PRO grazing
rn_icemac	100.0	%	MAC enhanced recruitment under ice
rn_kgrphy	.0118	L (m g Chl)$^{-1}$	light absorption in blue-green for DIA
	.0257	L (m g Chl)$^{-1}$	light absorption in blue-green for MIX
	.0257	L (m g Chl)$^{-1}$	light absorption in blue-green for COC
	.0696	L (m g Chl)$^{-1}$	light absorption in blue-green for PIC
	.0257	L (m g Chl)$^{-1}$	light absorption in blue-green for PHA
	.0657	L (m g Chl)$^{-1}$	light absorption in blue-green for FIX
rn_kmfbac	0.025e-9	mol L^{-1}	K_m for Fe in DOC remineralisation by bacteria
rn_kmfphy	40.e-9	mol L^{-1}	K_m^{Fe} for DIA
	25.e-9	mol L^{-1}	K_m^{Fe} for MIX
	25.e-9	mol L^{-1}	K_m^{Fe} for COC
	10.e-9	mol L^{-1}	K_m^{Fe} for PIC
	25.e-9	mol L^{-1}	K_m^{Fe} for PHA
	40.e-9	mol L^{-1}	K_m^{Fe} for FIX
rn_kmhnit	0.1e-6	mol L^{-1}	K_m^{NH4} nitrification
rn_kmhphy	5.e-6	mol L^{-1}	K_m^{NH4} for DIA
	0.5e-6	mol L^{-1}	K_m^{NH4} for MIX
	0.5e-6	mol L^{-1}	K_m^{NH4} for COC
	0.1e-6	mol L^{-1}	K_m^{NH4} for PIC
	1.5e-6	mol L^{-1}	K_m^{NH4} for PHA
	0.3e-6	mol L^{-1}	K_m^{NH4} for FIX
rn_kmnphy	2.e-6	mol L^{-1}	K_m^{NO3} for DIA
	2.0e-6	mol L^{-1}	K_m^{NO3} for MIX
	2.0e-6	mol L^{-1}	K_m^{NO3} for COC
	2.0e-6	mol L^{-1}	K_m^{NO3} for PIC
	3.0e-6	mol L^{-1}	K_m^{NO3} for PHA
	13.0e-6	mol L^{-1}	K_m^{NO3} for FIX
rn_kmobac	1e-7	mol L^{-1}	K_m for DOC in DOC remineralisation by bacteria
rn_kmpbac	1e-7	mol L^{-1}	K_m for PO_4
rn_kmpphy	7.6e-6	mol L^{-1}	$K_m^{PO_4}$ for DIA

Continued on next page

Table 18 – continued from previous page

Parameter	Value	Units	Description
	12.2e-6	mol L^{-1}	$K_m^{PO_4}$ for MIX
	15.9e-6	mol L^{-1}	$K_m^{PO_4}$ for COC
	15.9e-6	mol L^{-1}	$K_m^{PO_4}$ for PIC
	97.6e-6	mol L^{-1}	$K_m^{PO_4}$ for PHA
	24.4e-6	mol L^{-1}	$K_m^{PO_4}$ for FIX
rn_kmsbsi	20e-6	mol L^{-1}	K_m for the Si/C ratio of DIA
rn_krdphy	.0056	L (m g Chl)$^{-1}$	light absorption in red for DIA
	.0098	L (m g Chl)$^{-1}$	light absorption in red for MIX
	.0098	L (m g Chl)$^{-1}$	light absorption in red for COC
	.0197	L (m g Chl)$^{-1}$	light absorption in red for PIC
	.0098	L (m g Chl)$^{-1}$	light absorption in red for PHA
	.0181	L (m g Chl)$^{-1}$	light absorption in red for FIX
rn_lyscal	10e-5	mol L^{-1}	inertia conc. for $CaCO_3$ dissolution
rn_mormac	0.020	d^{-1}	MAC mortality rate
rn_motmac	1.0481	-	temp. dependence of MAC mortality
rn_mumpft	0.44	d^{-1}	maximum growth rate DIA
	0.35	d^{-1}	maximum growth rate MIX
	0.70	d^{-1}	maximum growth rate COC
	0.26	d^{-1}	maximum growth rate PIC
	0.68	d^{-1}	maximum growth rate PHA
	0.046	d^{-1}	maximum growth rate FIX
rn_munfix	0.56	-	fraction of growth rate during N2fix relative to growth on NO3
rn_mutpft	1.0379	-	temp. dependence of BAC
	1.0400	-	temp. dependence of proto-zooplankton
	1.0242	-	temp. dependence of meso-zooplankton
	1.1165	-	temp. dependence of macro-zooplankton
	1.0680	-	temp. dependence of DIA
	1.0461	-	temp. dependence of MIX
	1.0132	-	temp. dependence of COC
	1.0611	-	temp. dependence of PIC
	1.0520	-	temp. dependence of PHA
	1.0623	-	temp. dependence of FIX
rn_nitnh4	0.79	d^{-1}	maximum nitrification rate
rn_qmaphy	2.e-7	-	maximum quota for Fe for all phyto
rn_qmiphy	4.0e-6	-	minimum quota for Fe for all phyto
rn_qopphy	8.6e-6	-	optimal quota for Fe for all phyto
rn_readsi	0.1	d^{-1}	max. DSi remin.

Continued on next page

Table 18 – continued from previous page

Parameter	Value	Units	Description
rn_remdsi	179831	d^{-1}	DSi remin.
rn_retdsi	-4366	d^{-1}	T. depend. DSi remin.
rn_resbac	0.10	d^{-1}	BAC respiration at 0°C
rn_reszoo	0.018	d^{-1}	MAC respiration at 0°C
	0.028	d^{-1}	MES respiration at 0°C
	0.010	d^{-1}	PRO respiration at 0°C
rn_resphy	0.012	-	fractional phytoplankton loss rate: DIA
	0.15	-	fractional phytoplankton loss rate: MIX
	0.15	-	fractional phytoplankton loss rate: COC
	0.15	-	fractional phytoplankton loss rate: PIC
	0.15	-	fractional phytoplankton loss rate: PHA
	0.15	-	fractional phytoplankton loss rate: FIX
rn_retbac	1.0494	-	temp. dependence of BAC respiration
rn_retzoo	1.0942	-	temp. dependence of MAC respiration
	1.0887	-	temp. dependence of MES respiration
	1.0897	-	temp. dependence of PRO respiration
rn_rhfphy	29.	-	maximum/minimum Fe uptake rate
rn_rivdic	1.	-	(1 - estuarine retention fraction) of river DIC
rn_rivdoc	1.	-	(1 - estuarine retention fraction) of river DOC
rn_rivpoc	0.55	-	(1 - estuarine retention fraction) of river POC
rn_rivpo4	1.	-	(1 - estuarine retention fraction) of river PO_4
rn_rivsil	1.	-	(1 - estuarine retention fraction) of river SIL
rn_rivfer	0.25	-	(1 - estuarine retention fraction) of river FER
rn_scofer	1.e-3	$(\text{mol L}^{-1})^{-0.6}\ \text{d}^{-1}$	scavenging of Fe
rn_scmfer	1.e-3	$(\text{mol L}^{-1})^{-0.6}\ \text{d}^{-1}$	minimum scavenging of Fe
rn_sedfer	1e-11	mol L^{-1}	coastal release of Fe
rn_sigzoo	0.70	-	fraction of MAC excretion as PO_4
	0.68	-	fraction of MES excretion as PO_4
	0.66	-	fraction of PRO excretion as DOM
rn_sildia	0.42e-6	mol L^{-1}	$K_m^{SiO_3}$ for diatoms
rn_singoc	0.0303	$\text{m}^2\ (\text{kg d})^{-1}$	Sinking rate parameter of POC_l, $CaCO_3$ and DSi
rn_snkgoc	0.6923	-	sinking rate parameter of POC_l,$CaCO_3$ and SiO_2
rn_snkpoc	3.0	m d^{-1}	sinking speed of POC_s
rn_thmphy	0.7	g mol^{-1}	maximum CHL:C ratio for DIA
	0.4	g mol^{-1}	maximum CHL:C ratio for MIX
	0.4	g mol^{-1}	maximum CHL:C ratio for COC
	0.4	g mol^{-1}	maximum CHL:C ratio for PIC
	0.5	g mol^{-1}	maximum CHL:C ratio for PHA

Continued on next page

Table 18 – continued from previous page

Parameter	Value	Units	Description
	0.3	g mol^{-1}	maximum CHL:C ratio for FIX
rn_unazoo	0.18	-	unassimilated fraction of phyto during MAC grazing
	0.3	-	unassimilated fraction of phyto during MES grazing
	0.13	-	unassimilated fraction of phyto during PRO grazing

References

J. I. Antonov, D. Seidov, T. Boyer, R. Locarnini, A. Mishonov, H. Garcia, O. Baranova, M. Zweng, and D. Johnson. *World Ocean Atlas 2009, Volume 2: Salinity*. NOAA Atlas NESDIS 69. U.S. Government Printing Office, Washington, D.C., 2010.

Olivier Aumont. Pisces biogeochemical model. Unpublished report, 2005. URL `http://ftp.legos.obs-mip.fr/pub/romsagrif/DATA`$_R OMS/papers/manuel_p isces.pdf$.

A. Beusen, A. Dekkers, A. Bouwman, W. Ludwig, and J. Harrison. Estimation of global river transport of sediments and associated particulate c, n, and p. *Global Biogeochemical Cycles*, 19(4), 2005.

E. Boyle, J. Edmond, and E. Sholkovitz. Mechanism of iron removal in estuaries. *Geochimica et Cosmochimica Acta*, 41(9):1313–1324, 1977.

E. Buitenhuis, P. van der Wal, and H. J. de Baar. Blooms of emiliana huxleyi are sinks of atmospheric carbon dioxide: a field and mesocosm study derived simulation. *Global Biogeochemical Cycles*, 15:577–587, 2001.

E. Buitenhuis, C. Le Quere, O. Aumont, G. Beaugrand, A. Bunker, A. Hirst, T. Ikeda, T. O'Brien, S. Piontkovski, and D. Straile. Biogeochemical fluxes through mesozooplankton. *Global Biogeochemical Cycles*, 20:GB2003, 2006. doi: 10.1029/2005GB002511.

E. Buitenhuis, T. Hashioka, and L. Quéré. Combined constraints on ocean primary production and phytoplankton biomass from observations and a model. *Global Biogeochemical Cycles*, 27:847–858, 2013.

E. T. Buitenhuis and R. Geider. A model of phytoplankton acclimation to iron-light colimitation. *Limnol. Oceanogr*, 55(2):714–724, 2010.

R. Chester. *Marine Geochemistry*. Unwin Hyman, 1990.

L. da Cunha, E. T. Buitenhuis, C. Le Quéré, X. Giraud, and W. Ludwig. Potential impact of changes in river nutrient supply on global ocean biogeochemistry. *Global Biogeochemical Cycles*, 21:GB4007, 2007. doi: 10.1029/2006GB002718.

M. Dai and J. Martin. First data on trace-metal level and behavior in 2 major arctic river-estuarine systems (ob and yenisey) and in the adjacent kara sea, russia. *Earth And Planetary Science Letters*, 131(3-4):127–141, 1995.

H. J. W. de Baar and J. T. M. D. Jong. Distributions, sources and sinks of iron in seawater. In *The Biogeochemistry of Iron in Seawater*, pages 123–153. John Wiley, 2001.

P. Döll and B. Lehner. Validation of a new global 30-min drainage direction map. *Journal Of Hydrology*, 258(1-4): 214–231, 2002.

T. Fichefet and M. A. Morales-Maqueda. Modelling the influence of snow accumulation and snow-ice formation on the seasonal cycle of the antarctic sea-ice cover. *Climate Dynamics*, 15(4):251–268, 1999.

H. E. Garcia, R. Locarnini, T. Boyer, J. Antonov, O. Baranova, M. Zweng, and D. Johnson. *World Ocean Atlas 2009, Volume 3: Dissolved Oxygen, Apparent Oxygen Utilization, and Oxygen Saturation*. NOAA Atlas NESDIS 70. U.S. Government Printing Office, Washington, D.C., 2010a.

H. E. Garcia, R. Locarnini, T. Boyer, J. Antonov, M. Zweng, O. Baranova, and D. Johnson. *World Ocean Atlas 2009, Volume 4: Nutrients (phosphate, nitrate, silicate)*. NOAA Atlas NESDIS 71. U.S. Government Printing Office, Washington, D.C., 2010b.

J. Harrison, N. Caraco, and S. Seitzinger. Global patterns and sources of dissolved organic matter export to the coastal zone: Results from a spatially explicit, global model. *Global Biogeochemical Cycles*, 19(4), 2005.

C. Jeandel, D. Ruiz-Pino, E. Gjata, A. Poisson, C. Brunet, E. Charriaud, F. Dehairs, D. Delille, M. Fiala, C. Fravalo, and J.C. Miquel. Kerfix, a time-series station in the southern ocean: a presentation. *Journal of Marine Systems*, 17(1-4):555–569, 1998.

T. D. Jickells, Z. S. An, K. K. Andersen, A. R. Baker, G. Bergametti, N. Brooks, J. J. Cao, P. W. Boyd, R. A. Duce, K. A. Hunter, H. Kawahata, N. Kubilay, J. laRoche, P. Liss, N. Mahowald, J. M. Prospero, A. J. Ridgwell, I. Tegen, and R. Torres. Global iron connections betwen desert dust, ocean biogechemistry, and climate. *Science*, 308:67–71, 2005.

E. Kalnay, M. Kanamitsu, R. Kistler, W. Collins, D. Deaven, L. Gandin, M. Iredell, S. Saha, G. White, J. Woollen, Y. Zhu, M. Chelliah, W. Ebisuzaki, W. Higgins, J. Janowiak, K. C. Mo, C. Ropelewski, J. Wang, A. Leetmaa, R. Reynolds, R. Jenne, and D. Joseph. The ncep/ncar 40-year reanalysis project. *Bulletin of the American Meteorological Society*, 77(3):437–471, 1996.

R. Key, A. Kozyr, C. Sabine, K. Lee, R. Wanninkhof, J. Bullister, R. Feely, F. Millero, C. Mordy, and T.-H. Peng. A global ocean carbon climatology: Results from glodap. *Global Biogeochemical Cycles*, 18:GB4031, 2004.

V. I. Kourzoun. *Atlas of World Water Balance*. UNESCO, 1977.

R. A. Locarnini, A. Mishonov, J. Antonov, T. Boyer, H. Garcia, O. Baranova, M. Zweng, and D. Johnson. *World Ocean Atlas 2009, Volume 1: Temperature*. NOAA Atlas NESDIS 68. U.S. Government Printing Office, Washington, D.C., 2010.

M. Lohan and K. Bruland. Importance of vertical mixing for additional sources of nitrate and iron to surface waters of the columbia river plume: Implications for biology. *Marine Chemistry*, 98(2-4):260–273, 2006.

W. Ludwig and J. L. Probst. River sediment discharge to the oceans: Present-day controls and global budgets. *American Journal of Science*, 298:265–295, 1998.

W. Ludwig, J. Probst, and S. Kempe. Predicting the oceanic input of organic carbon by continental erosion. *Global Biogeochemical Cycles*, 10(1):23–41, 1996a.

W. Ludwig et al. River discharges of carbon to the world's oceans: Determining local inputs of alkalinity and of dissolved and particulate organic carbon. *Comptes Rendus de l'Academie des Sciences - Serie IIA Sci. Terres Planetes*, 323(12):1007–1014, 1996b.

G. Madec. *NEMO ocean engine Note du pole de modélisation*, volume 27. Institut Pierre-Simon Laplace, Paris, 2008.

J.-M. Martin and M. Meybeck. Elemental mass-balance of material carried by major world rivers. *Marine Chemistry*, 7(3):173–206, 1979.

J.-M. Martin and M. Whitfield. The significance of the river input of chemical elements to the ocean. In *Trace Metals in Sea Water*, pages 265–296. Plenum, 1983.

M. Meybeck and R. A. River discharges to the oceans: An assessment of suspended solids, major ions, and nutrients. Technical report, U.N. Environ. Programme, 1997.

H. Ploug, M. Iversen, M. Koski, and E. Buitenhuis. Production, oxygen respiration rates and sinking velocity of copepod fecal pellets: Direct measurements of ballasting by opal and calcite. *Limnol. Oceanogr.*, 53:469–476, 2008.

M. C. Prather. Numerical advection by conservation of second-order moments. *Journal of Geophysical Research*, 91(D6):6671–6681, 1986.

J. L. Sarmiento, J. C. Orr, and U. Siegenthaler. A perturbation simulation of co_2 uptake in an ocean general-circulation model. *Journal of Geophysical Research-Oceans*, 97(C3):3621–3645, 1992.

S. Seitzinger, J. Harrison, E. Dumont, A. Beusen, and A. Bouwman. Sources and delivery of carbon, nitrogen, and phosphorus to the coastal zone: An overview of global nutrient export from watersheds (news) models and their application. *Global Biogeochemical Cycles*, 19(4), 2005.

E. Sholkovitz. Flocculation of dissolved fe, mn, al, cu, ni, co and cd during estuarine mixing. *Earth And Planetary Science Letters*, 41(1):77–86, 1978.

S. Smith, D. Swaney, L. Talaue-McManus, J. Bartley, P. Sandhei, C. McLaughlin, V. Dupra, C. Crossland, R. Buddemeier, B. Maxwell, and F. Wulff. Humans, hydrology, and the distribution of inorganic nutrient loading to the ocean. *Bioscience*, 53(3):235–245, 2003.

R. Timmermann, H. Goosse, G. Madec, T. Fichefet, C. Ethe, and V. Duliere. On the representation of high latitude processes in the orca-lim global coupled sea ice-ocean model. *Ocean Modelling*, 8(1-2):175–201, 2005.

P. Treguer, D. Nelson, A. Vanbennekom, D. Demaster, A. Leynaert, and B. Queguiner. The silica balance in the world ocean - a reestimate. *Science*, 268(5209):375–379, 1995.

R. Wanninkhof. Relationship between wind-speed and gas-exchange over the ocean. *Journal of Geophysical Research-Oceans*, 97(C5):7373–7382, 1992.

J. Wiedenmann, K. Creswell, and M. Mangel. Connecting recruitment of antarctic krill and sea ice. *Limnol. Oceanogr.*, 54(3):799–810, 2009.

D. A. Wolf-Gladrow, R. E. Zeebe, C. Klaas, A. Koertzinger, and A. Dickson. Total alkalinity: the explicit conservative expression and its application to biogeochmical processes. *Marine chemistry*, 106:287–300, 2007.